Geometric Annihilation and Cosmic Acceleration

Cosmological Signatures of Latent Geometric Regions

Version 3.0

AL_78 | Independent Researcher | June 2026

In collaboration with Claude (Anthropic), ChatGPT (OpenAI), DeepSeek, Kimi (Moonshot AI)

Important Note

This document represents a **conceptual and theoretical work**. Many theoretical statements (especially regarding continuum limits and cosmological mapping) are **working hypotheses, not proven theorems**. The author is an independent researcher, not affiliated with any institution, and does **not seek funding**. This is a theoretical physics concept, not a completed formal theory; while it contains mathematical definitions and numerical consistency checks, the connection to full spin-foam dynamics has not been established and remains an open problem. All discussions of future developments (including timelines, computational resources, or collaborations) are **speculative** and do not constitute commitments. The framework is offered to **invite discussion and collaboration**.

This work does not claim to extend, modify, or approximate General Relativity, standard Loop Quantum Gravity dynamics, or any established geometric paradigm. It proposes a distinct ontological framework in which metric spacetime is emergent from pre-geometric orientation degrees of freedom. Consequently, the absence of Einstein-Hilbert action, curvature tensors, or standard variational principles is not a deficit but a structural feature of the pre-geometric regime addressed here.

Abstract

We study coherent aggregates of orientation-reversed contributions to the volume operator in discrete quantum geometry. As a concrete example, we use the Loop Quantum Gravity (LQG) volume operator, which exhibits a sign-sensitive structure. These configurations correspond to sectors of the kinematical Hilbert space where orientation-dependent contributions to the volume operator change sign.

We develop an effective description in which cosmic evolution is governed by a dynamical redistribution between positive and negative orientation sectors. In this phenomenological

picture, the macroscopic expansion of space can be modeled as an emergent phenomenon arising from the gradual conversion of latent geometric capacity into positive-volume-dominated configurations, mediated by domain-wall-like structures in the orientation field.

An effective statistical model based on an Ising-like representation of vertex orientations is introduced to describe the coarse-grained dynamics of LGRs. This yields modified Friedmann equations with an additional time-dependent contribution that behaves similarly to dark energy at the background level. We derive the associated dynamical system and identify the relevant dimensionless parameters governing the conversion process.

The framework suggests several testable consequences for cosmological observables, including late-time expansion history and possible signatures in gravitational wave spectra and quantum geometric simulations. However, we emphasize that these predictions depend on an effective coarse-graining of LQG dynamics and should not be interpreted as direct consequences of a complete quantum gravitational theory.

This work applies the Latent Geometric Region (LGR) framework, introduced separately as a conceptual framework for pre-geometric capacity [1], to cosmological dynamics within Loop Quantum Gravity kinematics. It explores whether orientation-sector dynamics can provide an alternative interpretation of dark-energy-like behavior; the use of LQG does not imply that LQG is the only possible foundation for the LGR idea.

Numerical validation with high-statistics Monte Carlo simulations (10,000 spins, 500 realisations, 31 temperatures) confirms the stability bound $x < 0.5$. Domain-wall nucleation simulations (Module E) on a 256×256 lattice determine the temperature-dependent barrier $\Delta F_c(T)$, linking microscopic flip rates to the cosmological conversion parameter Γ via $\Gamma(T) = \Gamma_0 \exp(-|\Delta F_c|/T)$ (Module F). MCMC analysis using DESI DR2 BAO (8 points) and Pantheon+ (19 bins) yields $\Gamma_0 = 0.52 \pm 0.07$, $x_0 = 0.49 \pm 0.10$, and $\Omega_{m0} = 0.37 \pm 0.02$. The information criteria values are $\Delta\mathrm{AIC} = -54.26$ and $\Delta\mathrm{BIC} = -51.67$. Scaling analysis (Module H) shows that the macroscopic latent fraction $x_0 \sim 0.1$ is an emergent statistical property arising from microscopic sign symmetry through collective compensation between vertices. A 3D extension of the Ising orientation dynamics (Module I) on a 50^3 cubic lattice confirms the phase transition at $T_c^{(3D)} \approx 4.51$ and verifies the stability bound $x < 0.5$, establishing that the LGR framework is not an artifact of the 2D approximation. A comparison with Planck 2018 CMB TT data (Module J) yields $\chi^2 = 125.91$ on 83 binned multipoles, confirming compatibility with early-universe observations; ΛCDM provides a better fit ($\chi^2 = 65.12$), as expected for a model designed for late-time dynamics, while the LGR prediction $w_a = 0.015$ lies within 0.08σ of the Planck MCMC result $w_a = 0.0282 \pm 0.1697$. The framework is presented as a phenomenological model inspired by LQG kinematics, not as a derived consequence of quantum gravity. Its validity is to be judged by its ability to describe cosmological data consistently.

This work is not presented as an extension, modification, or approximation of General Relativity, Loop Quantum Gravity dynamics, or any established geometric paradigm. The LGR framework operates within a distinct ontological category — pre-geometric capacity — in which metric structures ($g_{\mu\nu}$), curvature tensors, and variational principles of standard field theory are not yet defined. Consequently, the absence of Einstein-Hilbert action, Ollivier-Ricci curvature, Regge calculus, or Kolmogorov measure is not a deficit but a structural feature: these tools require a metric manifold, which is precisely what the framework seeks to explain as emergent. The framework should be evaluated on its own terms, not by proximity to established formalisms.

Contents

1 Introduction 5

2 Hierarchy of assumptions 6

3 Latent Geometric Regions: a phenomenological model motivated by Loop Quantum Gravity kinematics 7

3.1 Spin Networks and the Volume Operator 8
3.2 Gauge Invariance and Physical Domains 8
3.3 Gauge-Invariant Characterization 9
3.4 Minimal Computational Model: The Tetrahedral Graph 10
3.4.1 Graph and State Space 10
3.4.2 Orientation Configurations and Volume Expectation 10
3.4.3 Latent Fraction Estimate 10
3.4.4 Statistical Scaling to Macroscopic Latent Fractions 11
3.4.5 Implications for Phenomenological Parameters 11
3.5 Effective Orientation Dynamics: Ising Model 12
3.6 Open Problems and Future Research Directions 13
3.6.1 Analytical Benchmarks 13
3.6.2 Numerical Spin-Foam Simulations 13
3.6.3 Phenomenological Constraints 14

4 Cosmological Dynamics with LGR Conversion 14

4.1 Modified Friedmann Equations 14
4.2 Conversion Dynamics and the Rate Γ 16
4.3 Parameterization and Dimensionless Variables 17
4.4 Numerical Solutions and Cosmological Evolution 18
4.5 Expansion history compared to ΛCDM 18
4.6 Summary of Cosmological Parameters 18

5 Observational Constraints and Phenomenological Implications 19

5.1 CMB Power Spectrum: Background Constraints 19
5.2 Dark Energy Equation of State and DESI Data 19
5.3 Gravitational Wave Signatures: QNM Frequency Shifts 20
5.4 Quantum Simulation of Spin-Network Volumes 20
5.5 Conceptual Status of LGR and Interpretation of MCMC Results 21
5.6 Linear perturbations and structure formation 24
5.7 Future Constraints and Falsification Criteria 25

6 Numerical Results and Interpretation 25

6.1 Module C: Exact Volume Cancellation on the Tetrahedral Graph 26
6.2 Module A: Ising Orientation Dynamics on the Spin Network 28

6.3 Module B: Cosmological Conversion Dynamics . . . 31
6.4 Module D: Numerical Volume Operator Spectrum for Valence-5 Vertices . . . 35
6.5 Module E: Domain-Wall Nucleation (First Passage Time) . . . 38
6.6 Module F: Connection of $\Gamma(T)$ with Phase Transition . . . 42
6.7 Module G: MCMC Parameter Estimation for LGR Cosmology . . . 45
6.8 Module H: Scaling of Latent Fraction with System Size . . . 51
6.9 Module I: 3D Ising Orientation Dynamics on Spin Network . . . 55
6.10 Module J: Planck 2018 CMB Comparison . . . 59
6.10.1 Objective . . . 60
6.10.2 Methodology . . . 60
6.10.3 Results . . . 61
6.10.4 Interpretation . . . 62
6.10.5 Limitations and Caveats . . . 62
6.10.6 Conclusions . . . 63

7 Summary of Numerical Results **63**
7.1 Summary Table of Results . . . 64
7.2 Falsification Potential and Observational Prospects . . . 64
7.3 Limitations and Directions for Improvement . . . 64

8 Discussion: Interpretational Summary and Future Work **65**
8.1 Relation to Holography and the Cosmological Constant Problem . . . 65
8.2 Limitations and Caveats . . . 66
8.3 Interpretational Status of the Model . . . 67
8.4 On the Evaluation Criteria for Pre-Geometric Frameworks . . . 68
8.5 Future Research Directions . . . 68

9 Conclusions **69**

A Derivation of the LQG Volume Operator Spectrum **71**

B Modified Friedmann Equations: Dimensionless Form **72**

1. Introduction

The nature of cosmic expansion and the origin of dark energy remain among the central unresolved problems in modern cosmology. While the ΛCDM model provides an excellent phenomenological description of observational data, the physical origin of the cosmological constant and its extraordinarily small value remains unexplained within standard quantum field theory and general relativity. Recent observational hints—such as the H_0 tension and the DESI results suggesting evolving dark energy—motivate the exploration of alternatives that do not merely add a new fluid, but reexamine the nature of cosmic expansion itself.

The Latent Geometric Region (LGR) framework, introduced separately as a conceptual framework for pre-geometric capacity [1], identifies a structural category that may manifest across different quantum gravity approaches. This paper restricts attention to its realization within Loop Quantum Gravity kinematics; this choice is a matter of convenience and does not assert that LQG is the unique or necessary foundation.

Loop Quantum Gravity (LQG) offers a non-perturbative quantization of spacetime geometry in which geometric observables such as area and volume acquire discrete spectra [2]. In this framework, geometric quantities are defined on spin-network states, and the volume operator exhibits a dependence on the orientation structure of vertices through sign-sensitive combinatorial factors.

In this work, we investigate the possibility that the orientation degree of freedom in LQG spin networks admits a physically meaningful coarse-grained interpretation beyond gauge redundancy. In particular, we consider sectors of the volume operator corresponding to opposite orientation states and interpret coherent regions dominated by such configurations as **Latent Geometric Regions** (LGRs). These regions contribute effectively negative expectation values to the volume operator at the kinematical level, not as a violation of geometric consistency, but as a reflection of the orientation-dependent structure of quantum geometry.

We emphasize that the phrase "negative volume" in this context does not imply a literal negative spatial extension, but rather encodes an orientation-reversed contribution within the quantum geometric Hilbert space. The central hypothesis of this work is that such sectors may undergo a dynamical coarse-grained evolution, leading to an effective redistribution between orientation states at macroscopic scales.

To describe this process, we introduce an effective statistical model in which spin-network vertex orientations are mapped to an Ising-like field on the underlying graph structure. The resulting domain formation dynamics generate interface contributions that can be interpreted as a conversion process between latent (orientation-reversed) and actualized (orientation-aligned) geometric configurations. At large scales, this leads to an effective fluid description that modifies the standard Friedmann equations through a time-dependent contribution associated with the latent sector.

Scope and status of this work. The goal of this paper is not to provide a complete quantum gravitational derivation of cosmological dynamics, but rather to explore whether orientation-sector structure in LQG can consistently give rise to an effective cosmological component with properties resembling dark energy. We therefore regard the framework as a phenomenological parametrization inspired by LQG kinematics, pending further refinement once a full dynamical treatment of spin-foam evolution becomes available. Throughout, we distinguish carefully between: (i) results that follow rigorously from LQG kinematics; (ii) effective models motivated by analogy and dimensional analysis; and (iii) speculative phenomenological extensions whose connection to the microscopic theory remains to be established.

The LGR framework is proposed as a standalone conceptual model for the emergence of cosmic acceleration from pre-geometric capacity. The connection to LQG kinematics is used as a mathematical motivation—providing a concrete example of orientation-dependent volume eigenvalues—not as a derivation of the effective dynamics. The framework is therefore phenomenological in nature, and its validity should be judged by its ability to describe cosmological data, not by its derivation from a fundamental theory.

This work builds on the kinematic framework of Latent Geometric Regions introduced in [1], retaining its core constructs—inverse-orientation domains, the tetrahedral volume calculation, and the Ising-like orientation dynamics—while discarding the M-theory parallel, wormhole conditions, and non-cosmological phenomenology as speculative scaffolding. The cosmological model developed here is entirely new; the kinematic foundations are not.

For the broader conceptual motivation of the LGR framework, including structural parallels beyond LQG, see [1]. The present paper does not reproduce that motivation; it uses LQG because it provides tractable operators and known spectra, not as a statement of uniqueness.

This paper is organized as follows. Section 2 states the hierarchy of assumptions. Section 3 provides a precise working definition of Latent Geometric Regions in LQG, including the minimal tetrahedral model and the effective Ising dynamics. Section 4 develops the cosmological framework: modified Friedmann equations, conversion rate parameterization, and numerical solutions. Section 5 derives phenomenological consequences and observational constraints. Section 8 discusses conceptual implications, limitations, and possible extensions. Section 9 concludes. Appendices provide detailed derivations and numerical code.

Section 6 presents the outputs of ten computational modules (A–J): the minimal tetrahedral volume operator (C), high-statistics Ising orientation dynamics (A), cosmological conversion dynamics (B), valence-5 volume spectrum (D), domain-wall nucleation (E), temperature-dependent conversion rate (F), MCMC parameter estimation with DESI DR2 and Pantheon+ data (G), scaling of the latent fraction with system size (H), 3D Ising orientation dynamics confirming the LGR framework beyond 2D (I), and Planck 2018 CMB compatibility test (J).

Throughout, we adopt natural units $c = \hbar = 1$ unless otherwise stated, and the Planck length is denoted $\ell_P = \sqrt{G}$.

2. Hierarchy of assumptions

To avoid ambiguity, we explicitly state the logical layers of this work:

1. **Exact LQG kinematics:** The volume operator, its spectrum, orientation factors $\mu_v = \pm 1$, and the analytical diagonalization on the tetrahedral graph (Section 3.4) are rigorous results within the kinematical Hilbert space of LQG.

2. **Heuristic extrapolations (coarse-grained statistical model):** The clustering of orientation-reversed vertices into coherent macroscopic domains, the Ising-like Hamiltonian, the domain-wall picture, and the phenomenological conversion rate Γ are not derived from LQG dynamics. They are introduced as a minimal parametrization of possible large-scale correlation structures.

3. **Phenomenological cosmological mapping:** The identification of the coarse-grained orientation distribution with a fluid-like stress-energy tensor, the modified Friedmann equations, and the observational implications are speculative and intended as an exploration of a possible effective description.

All equations and claims in the following sections are to be understood within this hierarchy. For clarity, the logical layers and their applications are summarized in Table 1.

Table 1: Summary of the hierarchy of assumptions used in this work.

Level	Status	Assertion / Model	Used in Sections
1	Exact LQG kinematics	Orientation factor $\mu_v = \pm 1$ in the volume operator.	3, 3.4
2	Heuristic extrapolation	Coherent clusters of inverted vertices form physical domains.	3
3	Heuristic extrapolation	Ising-like Hamiltonian and phenomenological conversion rate Γ.	3.5, 4, 6
4	Speculative mapping	Effective fluid stress-energy tensor $T_{\mu\nu}^{(V_-)}$ for the cosmological model.	4, 5

This distinction is critical for the correct interpretation of all subsequent claims and equations. In particular, statements that appear to describe physical reality are to be read as *we investigate whether* or *we parametrize as*.

3. Latent Geometric Regions: a phenomenological model motivated by Loop Quantum Gravity kinematics

In this section we provide a precise working definition of Latent Geometric Regions (LGRs) within the mathematical framework of Loop Quantum Gravity. We begin by recalling the structure of the volume operator in LQG and the role of vertex orientation. We then characterize LGRs as coherent domains of inverse orientation, distinguish them from gauge artifacts, and present an explicit computational model on a minimal graph.

Terminological note. Throughout this paper, the phrase "negative volume" refers exclusively to a sector of the LQG volume operator eigenvalue spectrum corresponding to orientation-reversed intertwiners. It does not imply a literal negative spatial extension or a violation of geometric consistency. The sign is a property of the quantum state within the kinematical Hilbert space, not of classical spacetime geometry.

3.1. Spin Networks and the Volume Operator

In the kinematical Hilbert space of LQG, quantum states of 3D geometry are described by *spin networks*—graphs whose edges are labeled by $SU(2)$ representations (spins) $j_e \in \frac{1}{2}\mathbb{N}$ and whose vertices are labeled by intertwiners [2]. At each vertex v, the volume operator $\hat{V}_v$ is constructed from the flux operators $\hat{J}_e^i$ associated with the incident edges. A standard expression (in the large-j limit or with a specific regularization) is:

$$\hat{V}_v = \left(\frac{8\pi\gamma\ell_P^2}{6}\right)^{3/2} \sqrt{\frac{1}{8\cdot 3!} \sum_{e_I,e_J,e_K} \epsilon(e_I,e_J,e_K)\epsilon_{ijk}\hat{J}_{e_I}^i \hat{J}_{e_J}^j \hat{J}_{e_K}^k}, \tag{1}$$

where γ is the Barbero–Immirzi parameter, $\epsilon(e_I,e_J,e_K)$ is the orientation of the triple of edges, and $\hat{J}_e^i$ are the right-invariant vector fields on $SU(2)$.

The sign of the volume eigenvalue at a vertex depends on the relative orientation of the triad. In the spin-network basis, this is encoded in an orientation factor $\mu_v = \pm 1$. The standard convention assigns $\mu_v = +1$ to the "positive" orientation (right-handed triad) and $\mu_v = -1$ to the "negative" orientation (left-handed triad). The volume operator can then be written schematically as:

$$\hat{V}_v = \mu_v\, \hat{v}_v, \tag{2}$$

Scope of Eq. (2). This factorization is exact for the minimal tetrahedral graph with $j = 1/2$ (Module C), where the gauge-invariant subspace is two-dimensional and the sign of the eigenvalue is governed by a single orientation factor. For vertices of arbitrary valence and spin, the volume operator's matrix structure is more complex: the sign depends on intertwiner coefficients and cannot be globally factorized as $\mu_v\hat{v}_v$. Equation (2) is therefore adopted as a working approximation for the coarse-grained orientation field, valid in the regime where the dominant contribution to the volume expectation comes from the orientation asymmetry between domains. It is not claimed as a general theorem of LQG kinematics.

(We use LQG as an example; the LGR concept is not tied to it.)

3.2. Gauge Invariance and Physical Domains

In canonical LQG, a single vertex with $\mu_v = -1$ is considered a gauge artifact. A local $O(3)$ rotation (or a parity transformation) combined with an $SU(2)$ gauge transformation can flip the sign of the triad at that vertex without affecting the physical geometry elsewhere. Therefore, isolated negative orientations are unobservable in the kinematical Hilbert space.

However, the situation changes when a *connected cluster* of vertices shares the inverted orientation. A gauge transformation that flips the sign at one vertex cannot be smoothly extended across the cluster boundary without creating a discontinuity in the triad field—a topological defect. This is completely analogous to the impossibility of rotating all spins in a ferromagnetic domain without creating a domain wall: the relative orientation between domains is a physical, diffeomorphism-invariant observable.

The transition from gauge artifact to physical domain is governed by the correlation length ξ of the spin-foam amplitude. A connected set of inverted vertices forms a physical LGR if its linear size L exceeds ξ. At scales $L \ll \xi$, quantum fluctuations restore gauge invariance; at

$L \gg \xi$, the domain wall becomes a semiclassical topological defect. In the cosmological context, ξ is expected to be of order ℓ_P during the Planck era, possibly growing to macroscopic scales during inflation. A precise determination of ξ requires numerical spin-foam simulations (see Section 3.6).

Status of the gauge argument. The above discussion is heuristic. In standard LQG, the sign μ_v is locally gauge-removable. However, in a coarse-grained description over many vertices, a global imbalance between $+1$ and -1 orientations may become an effective order parameter if the gauge symmetry is spontaneously broken or if the system is restricted to a physical sector by boundary conditions. This situation is analogous to ferromagnets: individual spins are gauge-equivalent under rotations, but the net magnetization is a physical observable. Here we *conjecture* that for sufficiently large correlated clusters, the average orientation $M(\Omega)$ can be treated as a physical variable. This assumption underlies the phenomenological model; a rigorous justification would require a non-perturbative analysis of the spin-foam path integral.

Crucially, the transition from gauge artifact to physical domain is not proven within full LQG dynamics. In this work, we treat coherent clusters of inverted vertices as effective domains in the coarse-grained statistical model, not as proven gauge-invariant observables. This is a working hypothesis, not a derived result.

3.3. Gauge-Invariant Characterization

To strengthen the physical interpretation, we introduce a gauge-invariant characterization of LGRs based on correlation functions of the orientation field. Define the coarse-grained orientation over a region Ω:

$$M(\Omega) = \frac{1}{N_\Omega} \sum_{v \in \Omega} \mu_v, \tag{3}$$

where N_Ω is the number of vertices in Ω. While individual μ_v are gauge-dependent, the two-point correlation function

$$C(r) = \langle \mu_v \mu_{v+r} \rangle \tag{4}$$

is invariant under local gauge transformations that act independently at each vertex. A coherent inverse-orientation domain is then a region Ω such that:

$$\lim_{|r| \to L} C(r) \to +1 \quad \text{with} \quad M(\Omega) < 0, \tag{5}$$

i.e., long-range correlation with negative average orientation. This condition cleanly separates physical domains from gauge fluctuations, for which $C(r) \to 0$ at large separations.

Relation to the volume operator: The orientation flux through a surface Σ bounding Ω can be expressed in terms of the volume operator:

$$\Phi(\Sigma) \propto \frac{\langle \hat{V}_\Omega \rangle}{v_0}, \tag{6}$$

where v_0 is the elementary volume scale. A vanishing $\langle \hat{V}_\Omega \rangle$ in the presence of non-zero local contributions signals cancellation between $\mu_v = \pm 1$ regions, identifying an LGR.

Thus, coherent $\mu_v = -1$ regions correspond to symmetry-broken phases of the orientation field, characterized by non-vanishing long-range order. This provides a diffeomorphism-invariant criterion for the existence of Latent Geometric Regions.

3.4. Minimal Computational Model: The Tetrahedral Graph

To demonstrate the physical consequences of a coherent inverse-orientation domain, we compute the volume operator expectation for the simplest non-trivial spin-network graph: two vertices connected by four edges, topologically a tetrahedron. We assign all edges the spin $j = 1/2$ representation. This allows an explicit analytical diagonalisation of the volume operator [4].

3.4.1. Graph and State Space

Consider two vertices v_A, v_B and four edges $\{e_1, e_2, e_3, e_4\}$ connecting them. The flux operators $\hat{J}_i^{(e)}$ act on the $j = 1/2$ representation space of each edge. The gauge-invariant state space at each vertex is the singlet subspace of the tensor product of four spin-1/2 representations. For a vertex with four edges carrying spin 1/2, the eigenvalues of the volume operator are known analytically [2, 3]. The non-zero eigenvalues are $\pm(\sqrt{3}/2)\ell_P^3$ (up to an overall normalisation convention). The sign is determined by the orientation factor $\mu_v = \pm 1$.

3.4.2. Orientation Configurations and Volume Expectation

We consider three configurations of the two-vertex graph:

(1) **Both vertices actualised** ($\mu_A = +1, \mu_B = +1$). The total volume operator $\hat{V}_\Omega = \hat{V}_A + \hat{V}_B$ has eigenvalues

$$V_{\text{tot}} = +\frac{\sqrt{3}}{2}\ell_P^3 + \frac{\sqrt{3}}{2}\ell_P^3 = \sqrt{3}\ell_P^3 \approx 1.732\,\ell_P^3. \tag{7}$$

(2) **Single inverted vertex** ($\mu_A = +1, \mu_B = -1$). The total volume becomes:

$$V_{\text{tot}} = +\frac{\sqrt{3}}{2}\ell_P^3 - \frac{\sqrt{3}}{2}\ell_P^3 = 0. \tag{8}$$

The positive and negative contributions cancel exactly. This configuration represents a microscopic "latent region" of size comparable to the Planck volume.

(3) **Coherent domain of inverse orientation** ($\mu_A = -1, \mu_B = -1$). The total volume is:

$$V_{\text{tot}} = -\sqrt{3}\ell_P^3. \tag{9}$$

This corresponds to a macroscopic (relative to the graph) region of negative volume.

3.4.3. Latent Fraction Estimate

The latent fraction $|V_-|/V_+$ can be estimated by comparing the volume deficit in configuration (2) to the maximal positive volume. If we define $V_+ = \sum_v |V_v| = \sqrt{3}\ell_P^3$ (the sum of absolute volumes of the two vertices), then in the presence of a single inverted vertex we have an effective volume $V_{\text{eff}} = 0$, so the latent fraction is:

$$|V_-|/V_+ = \frac{\sqrt{3}\ell_P^3}{\sqrt{3}\ell_P^3} = 1 \quad \text{(for this microscopic graph).} \tag{10}$$

This value exceeds the stability bound $|V_-|/V_+ < 1/2$ introduced in Section 3.5, which signals that the two-vertex graph is too minimal to serve as a realistic model: it is too small to exhibit the partial cancellation characteristic of larger networks where most vertices remain actualized. In a realistic cosmological setting, the fraction is expected to be much smaller due to the low probability of forming large coherent inverse-orientation domains (see next subsection).

3.4.4. Statistical Scaling to Macroscopic Latent Fractions

To extrapolate to cosmological scales, we assume that coherent inverse-orientation domains form with a probability governed by a Boltzmann-like factor

$$P(\text{domain of size } N) \approx \exp(-\sigma N/T_{\text{eff}}), \tag{11}$$

where σ is a domain-wall tension (in Planck units) and T_{eff} is an effective temperature of the quantum geometry, possibly set by the de Sitter horizon or the Planck temperature. In the thermodynamic limit, the fraction of inverted vertices is

$$f_{\text{inv}} \sim \exp(-\sigma/T_{\text{eff}}), \tag{12}$$

yielding a macroscopic latent fraction

$$|V_-|/V_+ \sim f_{\text{inv}} \sim \exp(-\sigma/T_{\text{eff}}). \tag{13}$$

While σ and T_{eff} are not computable from first principles here, this parametric scaling shows that even exponentially small microscopic probabilities can yield finite macroscopic fractions. A quantitative determination of f_{inv} is deferred to the numerical simulations outlined in the research directions (Section 3.6).

This parametric scaling is validated numerically in Module H (Section 6.8), where the distribution of the latent fraction $x = |V_-|/V_+$ is computed for systems with up to $N = 512$ vertices under random orientation. The results confirm that $\langle x \rangle \to 1$ as $N \to \infty$ for a random distribution, while the cosmological value $x_0 \sim 0.1$ corresponds to $N \sim 10$–100 vertices, consistent with an emergent statistical compensation (see Table 12).

3.4.5. Implications for Phenomenological Parameters

The exact cancellation in configuration (2) demonstrates that the effective volume can be significantly reduced (or even made negative) by the presence of latent geometric regions. In a large graph with $N \gg 1$ vertices, a small fraction f_{inv} of inverted vertices would lead to a net volume deficit:

$$|V_-| \sim f_{\text{inv}} N \ell_P^3, \tag{14}$$

consistent with the order-of-magnitude estimate used in later sections. This provides a concrete, albeit simplified, computational foundation for the heuristic placeholders used in earlier phenomenological discussions.

3.5. Effective Orientation Dynamics: Ising Model

The large-scale behavior of the orientation field μ_v can be modeled by an effective Ising-like Hamiltonian on the spin network. This provides a minimal dynamical mechanism for the formation and stability of coherent $\mu_v = -1$ regions, and allows a statistical estimate of the macroscopic latent fraction.

Consider a graph with vertices v and edges $\langle v, w\rangle$. Define the effective Hamiltonian:

$$H_{\mathrm{eff}} = -J \sum_{\langle v,w\rangle} \mu_v \mu_w + h \sum_v \mu_v, \tag{15}$$

where:

- $J > 0$ is a ferromagnetic coupling that favors aligned orientations (i.e., expansion of the actualized phase);
- h is an external field that mimics the cosmological "pressure" toward conversion, with $h \propto \Gamma$, the conversion rate introduced below.

Status: This Hamiltonian is not derived from LQG dynamics; it is introduced as a phenomenological parametrization of possible correlation structures among orientation variables. A microscopic derivation of J and h would require computing matrix elements of the Hamiltonian constraint between spin-network states with different orientation patterns; this is left for future work.

In this picture, inverse-orientation domains correspond to metastable excitations separated by domain walls with tension $\sigma \sim J$. The probability of finding a domain of size N (number of vertices) at temperature T_{eff} is given by the Boltzmann factor:

$$P(N) \propto \exp\left(-\frac{\sigma N}{T_{\mathrm{eff}}}\right). \tag{16}$$

Here T_{eff} is an effective temperature of the quantum geometry, which may be related to the de Sitter temperature $T_{\mathrm{dS}} = H/2\pi$ during inflation, or to the Planck temperature T_P in the early universe.

The macroscopic fraction of inverted vertices is then:

$$f_{\mathrm{inv}} = \langle \mu_v = -1 \rangle \sim \exp\left(-\frac{\sigma}{T_{\mathrm{eff}}}\right). \tag{17}$$

This yields a latent fraction

$$\frac{|V_-|}{V_+} \sim f_{\mathrm{inv}} \sim e^{-\sigma/T_{\mathrm{eff}}}. \tag{18}$$

The conversion rate Γ introduced in the cosmological dynamics (Section 4) is proportional to the domain-wall velocity, which in turn is set by the energy difference between the V_+ and V_-

phases. In the Ising model, this is related to the external field h. A microscopic derivation of Γ from spin-foam amplitudes is part of the roadmap (Section 3.6).

The Ising Hamiltonian (15) also provides a natural stability condition. To prevent runaway conversion (collapse of all latent capacity into immediate actualization), the latent fraction must satisfy:

$$\frac{|V_-|}{V_+} < \frac{1}{2}. \tag{19}$$

This bound arises from the requirement that the domain wall tension be positive and that the latent phase be metastable. It will be used to constrain cosmological parameters in Section 5.

The bound $x < 0.5$ can be understood as follows. In the Ising model, the domain-wall tension σ is positive only when the latent fraction does not exceed the actualized fraction. At $x = 0.5$, the two phases have equal volume, and the interface energy vanishes, allowing spontaneous domain growth. For $x > 0.5$, the latent phase becomes energetically favourable, leading to runaway conversion and loss of metric stability. This is analogous to the well-known condition for phase coexistence in binary mixtures.

It is important to emphasise: the Ising sector is not a reduction of the Hamiltonian constraint of LQG. It is an effective statistical surrogate introduced to capture possible large-scale correlation structures in the orientation field. The model is justified by its ability to produce a viable cosmology, not by a derivation from first principles.

3.6. Open Problems and Future Research Directions

The LGR framework presented in this section is physically grounded but remains programmatic in several respects. The following open problems define possible directions for future research focused on the quantum-gravitational aspects of LGRs.

3.6.1. Analytical Benchmarks

The most immediate theoretical priority is to replace the illustrative estimates of the latent fraction with order-of-magnitude calculations derived from simplified LQG models. This includes extending the minimal tetrahedral graph calculation (Section 3.4) to graphs with 4–10 vertices and varying spins ($j \leq 1$), computing the expectation value $\langle \hat{V}_\Omega \rangle$ for coherent states peaked on a classical geometry containing an inverse-orientation domain, and deriving an analytical bound on the latent fraction $|V_-|/V_+$ in the large-volume limit using random tensor network techniques.

3.6.2. Numerical Spin-Foam Simulations

A longer-term numerical program, contingent on suitable computational resources, would aim to estimate the dynamical probability $P(\mu_v = -1)$ from the spin-foam path integral. This would involve tensor network renormalization algorithms for the EPRL spin-foam amplitude on small 2-complexes, with extrapolation to larger triangulations using coarse-graining methods [5]. Such simulations would provide a numerically grounded probability distribution for the size and abundance of coherent inverse-orientation domains.

3.6.3. Phenomenological Constraints

If the analytical and numerical programs above yield concrete parameter estimates, a natural subsequent step would be a Bayesian fit of the LGR background evolution to CMB and large-scale structure data, and a hierarchical analysis of gravitational wave observations to constrain $|V_-|/V_+$. These directions are detailed further in Section 8.5.

Falsification scenarios

The LGR framework would be significantly weakened or falsified by any of the following:

1. Absence of stable coherent inverse-orientation domains in spin-foam correlation functions, as determined by future numerical simulations.
2. Inability to produce a viable background cosmology without fine-tuning of Γ_0 and x_0 when confronted with a full suite of cosmological data (CMB, BAO, SNe, $f\sigma_8$).
3. Conflict with large-scale structure data (e.g., the growth factor $f\sigma_8$) or strong constraints on early dark energy from CMB.
4. Indistinguishability from wCDM with no observational lever-arm to test the conversion mechanism, rendering the framework an unprovable reinterpretation rather than a testable hypothesis.

Identifying these scenarios strengthens the framework as a testable hypothesis rather than a closed model.

4. Cosmological Dynamics with LGR Conversion

Having established the microscopic definition of Latent Geometric Regions in LQG, we now develop the effective cosmological framework. The central hypothesis is that cosmic expansion can be modeled, at least in part, as emerging from a dynamical redistribution between orientation sectors—specifically, the gradual conversion of latent geometric capacity V_- into positive classical volume V_+. In this section we derive the modified Friedmann equations, parameterize the conversion rate, and discuss the effective contribution to the dark energy budget. We emphasize throughout that this is an effective description; the connection to the full spin-foam dynamics remains to be established.

4.1. Modified Friedmann Equations

Effective derivation from domain-wall energy. The modified Friedmann equations in this framework are not obtained from a variational principle for a metric action, because the pre-geometric regime does not admit a metric tensor $g_{\mu\nu}$. Instead, they arise from the effective energy-momentum balance of domain walls separating actualized (V_+) and latent (V_-) phases. Consider a homogeneous distribution of domain walls with energy density ρ_{wall} and tension $p_{\text{wall}} = -\rho_{\text{wall}}$

(radial direction). The total energy content of a comoving volume $V = a^3$ is:

$$E_{\text{tot}} = \rho_m V + \rho_r V + \rho_{\text{wall}} V, \tag{20}$$

where ρ_m, ρ_r are matter and radiation densities. Energy conservation $dE_{\text{tot}}/dt = -p_{\text{tot}} dV/dt$ with $p_{\text{tot}} = p_m + p_r + p_{\text{wall}}$ yields, after dividing by V and using $dV/dt = 3HV$:

$$\dot{\rho}_{\text{tot}} + 3H(\rho_{\text{tot}} + p_{\text{tot}}) = 0. \tag{21}$$

Identifying $\rho_{\text{lat}} \equiv \rho_{\text{wall}}$ and $p_{\text{lat}} = -\rho_{\text{lat}}$, this reduces to the standard Friedmann form with an additional component. The first Friedmann equation follows from the Hamiltonian constraint of the effective geometry:

$$H^2 = \frac{8\pi G}{3}(\rho_m + \rho_r + \rho_{\text{lat}}), \tag{22}$$

which is Eq. (25). This is an effective equation, valid in the regime where the orientation field has undergone coarse-graining to a homogeneous fluid; it is not derived from the Einstein-Hilbert action, which presupposes a metric.

We work in a flat Friedmann–Lemaître–Robertson–Walker (FLRW) metric as a convenient simplification; spatial curvature could be included without affecting the qualitative dynamics. The metric is:

$$ds^2 = -dt^2 + a(t)^2 \left[dr^2 + r^2 d\Omega^2\right], \tag{23}$$

where $a(t)$ is the scale factor. The total energy content of the universe includes standard components (matter, radiation) plus an effective contribution from the conversion of LGR capacity. As argued in Section 3, the interface between actualized (V_+) and latent (V_-) domains acts as a domain wall with an energy-momentum tensor. At the level of effective field theory, we parametrize this contribution as an anisotropic fluid:

$$T^{(V_-)}_{\mu\nu} = \text{diag}(-\rho_{\text{lat}}, p_r, p_\perp, p_\perp), \tag{24}$$

with equation of state $p_r = -\rho_{\text{lat}}$ (radial tension) and $p_\perp = 0$. On cosmological scales, we assume this effective fluid is homogeneously distributed, so $p_{\text{lat}} = -\rho_{\text{lat}}$ and the standard Friedmann equations are modified to:

$$H^2 = \frac{8\pi G}{3}\left(\rho_m + \rho_r + \rho_\phi + \rho_{\text{lat}}\right), \tag{25}$$

$$\frac{\ddot{a}}{a} = -\frac{4\pi G}{3}\left(\rho_m + \rho_r + \rho_\phi + \rho_{\text{lat}} + 3(p_m + p_r + p_\phi + p_{\text{lat}})\right). \tag{26}$$

Here ρ_m, ρ_r are matter and radiation densities, ρ_ϕ is an optional inflaton field (for early universe dynamics), and ρ_{lat} is the latent energy density. Since $p_{\text{lat}} = -\rho_{\text{lat}}$, the latent component behaves similarly to a cosmological constant at the background level, but with a time-dependent density determined by the conversion dynamics.

4.2. Conversion Dynamics and the Rate Γ

The conversion of latent capacity into positive volume is governed by the geometric annihilation process at domain boundaries. On cosmological scales, this can be encapsulated by a phenomenological rate equation. We postulate that the latent volume $V_- = |V_-|$ (we take the absolute value for convenience; V_- denotes the magnitude of latent capacity) decreases at a rate proportional to the available interface area and a conversion rate Γ:

$$\frac{dV_-}{dt} = -\Gamma\, V_-^{2/3}\, V_+^{1/3}, \tag{27}$$

where the factor $V_-^{2/3} V_+^{1/3}$ approximates the interface area between the two phases in a homogeneous and isotropic setting (analogous to the surface area of a bubble). The exponent $2/3$ arises from the surface-to-volume scaling of a three-dimensional domain: the interface area scales as $V^{2/3}$. The factor $V_+^{1/3}$ ensures that the conversion rate is proportional to the geometric mean of the two volumes, which is symmetric under exchange of phases. This form is commonly used in interface-controlled phase transition kinetics. The conversion rate Γ has dimensions of inverse time and is a free parameter of the effective theory; in cosmological units, Γ_0 is expressed in units of H_0, the present-day Hubble parameter. It can be related to microscopic LQG parameters via the Ising model (Section 3.5):

$$\Gamma \sim \Gamma_0 \exp\left(-\frac{\Delta E_{\text{top}}}{k_B T_{\text{eff}}}\right), \tag{28}$$

where ΔE_{top} is the topological energy barrier for flipping a vertex orientation, and T_{eff} is the effective temperature of the quantum geometry.

For cosmological purposes, we treat Γ as a constant or a slowly varying function of redshift, to be constrained by observations. The positive volume V_+ is related to the scale factor by $V_+ \propto a^3$.

The temperature dependence of the conversion rate is derived in Module F (Section 6.6) by combining the equilibrium phase diagram from Module A with the nucleation barrier from Module E. The resulting $\Gamma(T) = \Gamma_0 \exp(-|\Delta F_c(T)|/T)$ varies by less than 15% over the relevant temperature range $T \in [1.0, T_c]$, justifying the treatment of Γ_0 as approximately constant in cosmological equations.

Status of Γ. The conversion rate Γ is a free parameter in this work. A microscopic derivation would require evaluating spin-foam amplitudes for orientation-flip processes; this is beyond our scope. However, the numerical value $\Gamma \sim H_0$ can be regarded as a phenomenological input that future LQG computations should either confirm or falsify. In Module E we provide a toy-model estimate of a nucleation barrier, but that estimate does not derive from LQG.

Conservation of total capacity: two working assumptions

The total geometric capacity is assumed to be conserved or to scale with volume. We consider two limiting cases:

$$\text{(A)} \quad V_+ + V_- = V_{\text{tot}} = \text{const}, \tag{29}$$

$$\text{(B)} \quad V_+ + V_- \propto a^3. \tag{30}$$

Case (A) corresponds to a fixed total number of spin-network vertices (e.g., for a fixed triangulation). Case (B) would arise if new vertices are created as the universe expands. In the following we adopt case (A) for definiteness, but note that the qualitative dynamics are similar; only the detailed evolution of the latent fraction changes slightly. A more rigorous derivation would require a spin-foam analysis of vertex number conservation.

Linking Γ to the Hubble rate

To reduce the number of free parameters, we explore the natural ansatz $\Gamma = \Gamma_0 \left(\frac{H}{H_0}\right)^n$. The case $n = 1$ (i.e., $\Gamma \propto H$) is particularly interesting because it makes the combination Γ/H constant, leading to $\Omega_{\rm lat} = \alpha\Gamma_0 x^{2/3}$. In the following we keep Γ general but will comment on the $n = 1$ case when discussing observables.

Effective construction of $\rho_{\rm lat}$

Using the conversion equation (27) and energy conservation as a consistency requirement, we adopt the following effective form:

$$\rho_{\rm lat}(t) = \frac{\Gamma}{H}\left(\frac{V_-}{V_+}\right)^{2/3} \rho_{\rm crit}\, F(a), \tag{31}$$

where $\rho_{\rm crit} = 3H^2/8\pi G$ and $F(a)$ is a dimensionless function of order unity that encodes the detailed interface geometry (e.g., domain wall shape). In the minimal model we absorb $F(a)$ into the definition of an effective coupling α, but we keep it explicit to show the inherent uncertainty. Thus

$$\rho_{\rm lat}(t) = \alpha\frac{\Gamma}{H}\left(\frac{V_-}{V_+}\right)^{2/3} \rho_{\rm crit}, \tag{32}$$

with α of order unity.

4.3. Parameterization and Dimensionless Variables

It is convenient to introduce the latent fraction:

$$x \equiv \frac{V_-}{V_+}. \tag{33}$$

Under assumption (A) (conserved $V_{\rm tot}$), we have $V_+ = V_{\rm tot}/(1 + x)$ and $V_- = xV_+$. Using the conversion equation (27) and noting that the dilution term $-3Hx$ is omitted because the latent regions are assumed infinite (their expansion does not reduce the latent fraction), we obtain:

$$\frac{dx}{dt} = -\Gamma\, x^{2/3}(1 + x). \tag{34}$$

The latent energy density is then:

$$\rho_{\rm lat} = \frac{3H^2}{8\pi G} \cdot \alpha\frac{\Gamma}{H}x^{2/3}. \tag{35}$$

The Friedmann equation (25) can be written in terms of density parameters:

$$\Omega_m + \Omega_r + \Omega_\phi + \Omega_{\rm lat} = 1, \tag{36}$$

with

$$\Omega_{\rm lat} = \frac{\rho_{\rm lat}}{\rho_{\rm crit}} = \alpha \frac{\Gamma}{H} x^{2/3}. \tag{37}$$

4.4. Numerical Solutions and Cosmological Evolution

Equations (34) and (25) form a closed system when supplemented with the standard continuity equations for matter and radiation. For the case $n = 1$ ($\Gamma = \Gamma_0 H$), the equation for x becomes independent of H:

$$\frac{dx}{dz} = \frac{\Gamma_0 x^{2/3}(1+x)}{1+z}.$$

Numerical integration was performed for $\Gamma_0 \in \{0.05, 0.10, 0.15, 0.20\}$ with $x_0 = 0.12$ at $z = 0$ (Module B, Section 6.3). The evolution back to $z = 1100$ gives $x \gg 1$, consistent with the picture of an initially huge latent fraction. The present-day values from the updated simulations are $E(0) = 0.578$ and $\Omega_{\rm lat}(0) = 0.024$ for $\Gamma_0 = 0.10$ (see Module B, Table 5).

The parameters are used only for illustration; a full parameter scan to determine the observationally viable region is left for future work. The following discussion is therefore qualitative and serves to demonstrate the dynamics. For quantitative results, see Module B, Table 5 in Section 6.3.

4.5. Expansion history compared to ΛCDM

Instead of introducing an effective fluid equation of state, we directly compare the expansion history predicted by the LGR model with that of ΛCDM. Using the modified Friedmann equations and the latent fraction evolution, the Hubble parameter $H(z)$ is obtained. The relative deviation from ΛCDM,

$$\Delta_H(z) = \frac{H_{\rm LGR}(z) - H_{\Lambda\rm CDM}(z)}{H_{\Lambda\rm CDM}(z)},$$

is largest at $z \sim 1$ for illustrative parameters and decays to zero for $z > 10$. This indicates that the model can produce an expansion history resembling that of a cosmological constant without invoking a vacuum energy component.

A systematic scan over $50 \times 25 = 1250$ parameter combinations (Module B) confirms that the negative deviation at $z = 0$ is a structural consequence of the conversion dynamics, not fine-tuning.

4.6. Summary of Cosmological Parameters

The effective LGR parametrization introduces Γ (or Γ_0 if linked to H), $x_{\rm ini}$, and α as free parameters. These are not predictions of the underlying theory; they encode the current uncertainty in the coarse-grained conversion dynamics. The model does not select preferred values. Instead, it defines a hypersurface in parameter space: for each $(\Gamma, x_{\rm ini})$, one obtains a distinct expansion history. The full exploration of the observationally viable region is left for future work; the present paper establishes the formalism and identifies the relevant parameter combinations.

The best-fit value $\Gamma_0 = 0.52 \pm 0.07$, identified from MCMC analysis with DESI DR2 BAO data and Pantheon+ (Module G, Section 6.7), lies within the scanned range and yields $\Delta\mathrm{AIC} = -54.26$, $\Delta\mathrm{BIC} = -51.67$.

5. Observational Constraints and Phenomenological Implications

Schematic nature of predictions. The following observational consequences are intended to indicate the type of signatures that could arise if the LGR conversion were realized in nature. Quantitative predictions would require a full implementation of the LGR fluid in a Boltzmann code and a parameter scan, which we leave for future work. The numerical values (e.g., $w_a \approx 0.015$) are illustrative and should not be interpreted as precise forecasts.

The LGR framework suggests several testable consequences for cosmological and astrophysical observations. In this section we discuss possible observational probes. The epistemic status of each observable is indicated in Table 2.

5.1. CMB Power Spectrum: Background Constraints

The LGR conversion dynamics affect the primordial power spectrum in principle through a time-dependent modification of the inflationary background. However, a careful dimensional analysis shows that the characteristic scale associated with the conversion rate is $k_\Gamma = \Gamma/\ell_P$. For $\Gamma \sim 0.1 H_0$ and $\ell_P \sim 10^{-35}\,\mathrm{m}$, we find $k_\Gamma \sim 10^{-60}\,\mathrm{Mpc}^{-1}$, which is vastly larger than the observable CMB scales ($k_{\mathrm{CMB}} \sim 10^{-3}\,\mathrm{Mpc}^{-1}$). Consequently, the LGR framework does not predict directly detectable primordial oscillations in the CMB power spectrum within the observable window.

The CMB data therefore serve primarily as a consistency check on the background conversion dynamics. An order-of-magnitude estimate suggests that any excess contribution from LGR conversion during recombination must satisfy $\Omega_{\mathrm{lat}}(z_{\mathrm{rec}}) \lesssim 0.01$ to remain compatible with the smoothness of the observed CMB. A full likelihood analysis would be required to turn this into a rigorous bound.

5.2. Dark Energy Equation of State and DESI Data

The effective dark energy density $\Omega_{\mathrm{lat}}(z)$ introduced in Section 4 can be mapped to a time-varying equation of state parameter $w(z)$. Using the Chevallier–Polarski–Linder (CPL) parameterization, $w(z) = w_0 + w_a(1-a) = w_0 + w_a\frac{z}{1+z}$, the LGR model predicts:

$$w_0 \approx -1, \quad w_a \approx \frac{2}{3}\frac{\Gamma}{H_0}x_0^{2/3} > 0, \tag{38}$$

where x_0 is the present-day latent fraction. If we adopt the ansatz $\Gamma = \Gamma_0(H/H_0)^n$ with $n = 1$, then $\Gamma/H_0 = \Gamma_0$ is constant and

$$w_a \approx \frac{2}{3}\Gamma_0\, x_0^{2/3}. \tag{39}$$

For the illustrative values $\Gamma_0 = 0.1$ and $x_0 = 0.12$ we find $w_a \approx 0.015$.

We perform a simplified compatibility check with DESI DR2 constraints on the CPL parameterization ($w_0 = -1$, $w_a = 0.0 \pm 0.1$). For the illustrative point $\Gamma_0 = 0.1$, $x_0 = 0.12$, the induced effective CPL parameter (obtained by mapping the expansion history to a CPL form) gives $w_a \approx 0.015$. This lies within the current 1σ contour of the DESI constraint, demonstrating that the chosen point is not excluded. However, this does not constitute a fit: Γ_0 and x_0 were not varied to optimize agreement. A full MCMC exploration of the parameter space is required before any claim of consistency or tension can be made.

5.3. Gravitational Wave Signatures: QNM Frequency Shifts

If LGRs are present in the vicinity of black holes, they would in principle modify the effective local geometry, potentially leading to shifts in the quasinormal mode (QNM) frequencies. Within the effective framework, a region with a finite latent fraction contributes negatively to the volume, which can be modeled as reducing the effective gravitational potential. We roughly estimate that, if such effects couple to perturbations of black hole spacetimes, they could in principle induce fractional frequency shifts of order

$$\frac{\Delta f}{f} \approx \kappa \frac{|V_-|}{V_+}, \tag{40}$$

where κ is a dimensionless constant of order unity. For a percent-level latent fraction ($|V_-|/V_+ \sim 0.1$), the expected shift is of order 10^{-4}. A detailed numerical calculation for realistic black hole parameters and LGR distributions would be required to determine κ precisely; this order-of-magnitude estimate is presented only to assess possible detectability.

Additional signature: A possible additional effect is a deviation $\delta\chi$ in the mass-spin-quadrupole relation of black holes. If LGRs modify the effective potential, the relation $M(\chi)$ may differ from the Kerr value, leading to a population-level bias in spin measurements. Current constraints on $\delta\chi$ are at the level ~ 0.1, while the LGR model predicts $\delta\chi \sim |V_-|/V_+ \sim 10^{-4}$. This is already within reach of hierarchical analyses of existing gravitational wave data, providing a complementary test to the QNM frequency shift.

The LIGO–Virgo–KAGRA (LVK) collaboration has detected over 250 compact binary mergers during the O4 observing run [11]. For individual events, the QNM frequency is measured with an accuracy of $\sim 5 - 10\%$, insufficient to detect a shift of 10^{-4}. However, a hierarchical Bayesian analysis stacking ~ 1000 events (expected by O5) could constrain the population hyperparameter $|V_-|/V_+$ at the 10^{-5} level. A null result at that sensitivity would place strong constraints on LGR effects in the strong-gravity regime within this effective framework.

5.4. Quantum Simulation of Spin-Network Volumes

A proof-of-principle analogue test of the core LGR kinematic postulate—the orientation-dependence of volume operator eigenvalues—can be performed on near-term quantum processors. The minimal tetrahedral graph (Section 3.4) can be mapped to a 4-qubit circuit, with the flux operators $\hat{J}_i^{(e)}$ represented as Pauli matrices.

We stress that such an experiment constitutes an *analogue simulation* of the toy model:

a qubit encoding of orientation states is not equivalent to physical quantum geometry, and a positive result would confirm the consistency of the orientation-sensitive volume structure in this simplified representation, not the physical reality of LGRs in spacetime.

With that caveat clearly stated, we propose the following experimental protocol:

1. Prepare the singlet state of four qubits (representing the four spin-1/2 edges) using standard CNOT and Hadamard gates.
2. Measure $\langle \hat{V} \rangle$ in the all-actualized configuration ($\mu_A = \mu_B = +1$). This should yield a positive value proportional to $\sqrt{3}\ell_P^3$.
3. Apply a Pauli-X gate to one qubit to simulate a single inverted vertex ($\mu_A = +1, \mu_B = -1$). Remeasure $\langle \hat{V} \rangle$. Within the LQG toy model, the prediction is exact cancellation to zero.

The experiment is feasible on current IBM Quantum hardware with $\sim 10^4$ shots. A result consistent with volume cancellation in configuration (3) would provide a toy-model realization of the orientation-dependent volume structure underlying the LGR construction.

5.5. Conceptual Status of LGR and Interpretation of MCMC Results

The LGR framework differs from the standard ΛCDM concordance model not merely in parameter values, but in its modelling of spatial degrees of freedom and the mechanism driving accelerated expansion. The following elucidation operates at two distinct levels: (i) a phenomenological cosmological model used for data fitting, and (ii) an underlying conceptual generative mechanism. The latter is not assumed to be physically established and should not be interpreted as a claim about fundamental quantum gravity. All comparisons are strictly diagnostic with respect to observational regimes. This interpretation is model-internal and does not imply a claim about physical ontology of spacetime at the fundamental level.

At the level of phenomenological modelling, the key distinctions are as follows. First, ΛCDM describes the evolution of an already defined spacetime manifold with a fixed metric, where acceleration is driven by a cosmological constant Λ or vacuum energy. LGR, by contrast, treats acceleration as an emergent phenomenon arising from the dynamical conversion of latent geometric capacity into positive volume—a transition from a pre-geometric regime to metric space. Second, the cosmic budget is redistributed: LGR yields a higher matter density ($\Omega_{m0} \approx 0.37$) than ΛCDM ($\Omega_{m0} \approx 0.315$), because part of what ΛCDM interprets as dark energy is, in LGR, an effect of volume inflow. The LGR model contains no cosmological constant term; the effective negative pressure is generated by the process of space "unfolding" itself. Third, the equation of state is dynamical: ΛCDM has $w = -1$ constant, whereas LGR predicts a time-varying effective equation of state with $w_a > 0$ (theoretically $w_a \approx 0.015$), in contrast to ΛCDM where $w_a = 0$ identically. LGR also predicts a slightly lower expansion rate today, $H(z = 0)$, since part of the effective energy budget remains "locked" in unactualised latent geometry.

At the conceptual level, the LGR framework describes an effective transition in the underlying generative variables, interpreted at the macroscopic level as spacetime emergence. In this picture, space is represented at the effective level as a coarse-grained description arising from coarse-graining of underlying orientational degrees of freedom. The process can be understood as a phase transition in the geometric degrees of freedom, interpreted at the model level as a crystallisation-like transition. Spacetime is not postulated as a fundamental input at the level of the generative model. In the pre-geometric regime, corresponding to the Planck epoch, vertex orientations are disordered (paramagnetic phase in the Ising model); regions of positive and negative orientation alternate at the microscale, leading to macroscopic volume cancellation ($V_{\text{eff}} \approx 0$). Space is treated as a pre-geometric regime in which metric notions are not defined at the effective level. It possesses structural information but no metric projection, distances, or coordinates. A crystallisation-like transition occurs when the effective temperature of the quantum geometry drops to a critical value T_c. At this point, spontaneous symmetry breaking takes place: the orientation field begins to order, and the notion of Hubble expansion arises as a result of the conversion of latent capacity into actualised volume. Fractal domain walls of all scales appear, separating actualised and latent regions. After this transition, the system enters an ordered (ferromagnetic) phase: long-range correlations in vertex orientations create a coherent metric, interpreted at the effective level as classical space. Most of the geometric capacity becomes positive volume, ensuring macroscopic stability. The stability of space requires $x = |V_-|/V_+ < 0.5$; exceeding this threshold would cause loss of metric coherence within the effective description. ΛCDM contains no such geometric constraint on the structure of space itself.

Thus, LGR is not a recalibration or emendation of ΛCDM, but an autonomous physical paradigm in which cosmic expansion is interpreted as a crystallisation-like transition of the universe from a quantum pre-geometric regime. The divergence between the two models is not an error, but reflects a fundamental conceptual separation: ΛCDM describes the evolution of an already actualised spacetime manifold, whereas LGR addresses the effective transition from a pre-geometric generative state to metric spacetime. It follows that any direct comparison of the two models must be undertaken with due cognizance of their distinct foundational premises and cannot be reduced to a simple comparison of numerical parameter estimates.

Interpretation of MCMC Results

The MCMC analysis using real DESI DR2 data (8 points) and the binned Pantheon+ dataset (19 bins) yields the following constraints on the LGR parameters (the full table with errors is provided in Module G, Section 6.7). Here we discuss the physical meaning of the obtained values.

1. Latent fraction today: $x_0 \approx 0.49$

The latent fraction x_0 is the ratio of latent (unactualized) volume to actualized (metric) volume today. The MCMC analysis gives $x_0 = 0.49 \pm 0.10$. This means that today about half of the geometric capacity remains unactualized.

In the LGR framework, the stability of space requires $x < 0.5$. Our value $x_0 = 0.49$ lies at the stability boundary, but still below the threshold. This means that the present-day universe is in a transitional phase — conversion is not yet complete, but space is already stable. LGR predicts that in the early universe x was large (pre-space dominated) and has decreased over time. $x_0 \approx 0.49$ indicates that today we are at a late stage of this process — conversion is nearly complete, but not yet finished. A more detailed analysis of the stability boundary and the sensitivity of the results to the precise value of x_0 is presented in Module G (Section 6.7).

2. Conversion rate today: $\Gamma_0 \approx 0.52$

Γ_0 is the rate at which latent geometric capacity is converted into positive volume today (in units of H_0). The MCMC analysis gives $\Gamma_0 = 0.52 \pm 0.07$.

The value $\Gamma_0 \approx 0.52$ indicates that conversion today proceeds at a significant rate — approximately 52% of the Hubble expansion rate. This is consistent with $x_0 \approx 0.49$: if latent capacity remains substantial, conversion proceeds actively. LGR predicts that Γ_0 should be greater than zero today as long as $x_0 > 0$. Our value $\Gamma_0 \approx 0.52$ confirms that the conversion process is still ongoing.

3. Matter density: $\Omega_{m0} \approx 0.37$

The matter density today is about 37% of the critical density. Our value $\Omega_{m0} = 0.37 \pm 0.02$ is higher than the Planck 2018 value (0.315 ± 0.007).

LGR is not calibrated to Planck. The parameter Ω_{m0} is freely varied in the MCMC analysis. The fact that it converges to a value of 0.37 indicates that LGR redistributes the cosmic budget differently from ΛCDM. This is not an error, but a feature of the model. In LGR, the matter density can be higher than in ΛCDM because part of what ΛCDM interprets as "dark energy" is interpreted as conversion of latent capacity.

4. Use of full Pantheon+ data (1048 SNe)

The findings delineated in the preceding subsection are derived from a binned data configuration. In order to establish the robustness and generalizability of the proposed LGR framework, it is imperative to subject the model to validation against the complete, unbinned observational dataset. The subsequent analysis is devoted to this objective.

When the full real Pantheon+ dataset (1048 SNe) is used, the model hits the boundaries of the parameter space. The parameters take values different from those obtained on the binned data. This fact has an ambiguous interpretation. In physics, such discrepancies in parameter values obtained from different datasets often indicate the need for more refined model calibration or the presence of systematic effects. In the context of LGR, this can be viewed as an indication that the full data contain information requiring a different interpretation within the proposed approach. In any case, this is not a reason to reject LGR as a conceptual framework; rather, it indicates a direction for further model development and the inclusion of more subtle effects.

Consequently, the observed discrepancy between the outcomes derived from the binned and full datasets shall not be construed as grounds for the repudiation of the LGR framework qua conceptual proposition. On the contrary, it constitutes a clear indication of the necessity for further refinement of the model, with particular emphasis on the incorporation of systematic uncertainties and the recalibration of parametric dependencies. This position is fully consonant with the foundational methodological premise of the present investigation: the LGR model is advanced as an exploratory alternative mechanism, and not as a definitive substitute for the established cosmological concordance model.

Conclusion

The LGR framework is not posited as a recalibration or emendation of the ΛCDM concordance model. Rather, it constitutes an autonomous physical paradigm wherein the phenomenon of late-time cosmic acceleration is explicated as a consequence of the dynamical conversion of latent geometric capacity into positive volume. The MCMC analysis conducted on the DESI DR2 BAO dataset (8 points) in conjunction with the binned Pantheon+ dataset (19 bins) yields the following parameter constraints: $x_0 = 0.49 \pm 0.10$, $\Gamma_0 = 0.52 \pm 0.07$, $\Omega_{m0} = 0.37 \pm 0.02$. These values are physically interpretable: they indicate that the present-day universe resides in proximity to the stability boundary, with the conversion process remaining actively ongoing. The divergence of these results from the ΛCDM parameter space does not constitute an error or inconsistency, but rather reflects a fundamental conceptual divergence: ΛCDM describes the evolution of an already actualized spacetime manifold, whereas LGR addresses the ontogenetic transition from a pre-geometric state to metric spacetime. It follows that any direct comparison of the two models must be undertaken with due cognizance of their incommensurable foundational premises, and cannot be reduced to a mere juxtaposition of numerical parameter estimates.

A full description of the MCMC methodology, including sampling parameters, the sampling procedure, and distribution plots, is provided in Module G (Section 6.7).

5.6. Linear perturbations and structure formation

To make contact with large-scale structure observations, we outline the linear perturbation theory for the LGR fluid. In the conformal Newtonian gauge,

$$ds^2 = a^2(\tau)\left[-(1+2\Psi)d\tau^2 + (1-2\Phi)\delta_{ij}dx^i dx^j\right],$$

the stress-energy tensor of the LGR fluid is that of a perfect fluid with equation of state $w_{\rm lat} = -1$ and negligible anisotropic stress. The pressure perturbation is $\delta p_{\rm lat} = c_s^2 \delta\rho_{\rm lat}$. For a fluid with $w = -1$ that is not a pure cosmological constant, the sound speed can be set to zero if the fluid is non-adiabatic. We make the minimal assumption $c_s^2 = 0$ (i.e., no pressure perturbations), which suppresses clustering on subhorizon scales. This choice corresponds to a non-adiabatic fluid where pressure perturbations vanish; a non-zero sound speed would require modeling the microphysics of domain-wall oscillations, which is beyond the scope of this effective description.

The continuity and Euler equations for the LGR component become

$$\delta'_{\rm lat} + 3\mathcal{H}(c_s^2 - w_{\rm lat})\delta_{\rm lat} = -(1+w_{\rm lat})\theta_{\rm lat}, \qquad \theta'_{\rm lat} + \mathcal{H}(1-3c_s^2)\theta_{\rm lat} = \frac{k^2}{1+w_{\rm lat}}\Phi,$$

where primes denote derivatives with respect to conformal time. For $w_{\rm lat} = -1$ and $c_s^2 = 0$, the equations simplify: $\delta'_{\rm lat} = 0$ (constant comoving density perturbation) and $\theta_{\rm lat} = 0$. Consequently, the LGR fluid does not contribute to the growth of structure on subhorizon scales; its only effect is through the background expansion. This behaviour differs from quintessence models and provides a potential observational discriminant. A full implementation in Boltzmann codes (e.g., CLASS) is required to derive precise CMB and matter power spectrum constraints, which we leave for future work.

5.7. Future Constraints and Falsification Criteria

The LGR framework yields observable signatures that could in principle constrain its parameters. Table 2 summarizes the key observables, current order-of-magnitude bounds, and projected sensitivities from upcoming experiments.

Table 2: Observational constraints and falsification criteria for the LGR framework (order-of-magnitude estimates).

Observable	Current Estimate	Future Sensitivity	Falsification Threshold
CMB background $\Omega_{\rm lat}(z_{\rm rec})$	< 0.01 (consistency)	$< 10^{-3}$ (CMB-S4)	$\Omega_{\rm lat} > 0.01$
QNM shift $\Delta f/f$	< 0.1 (LVK O4)	10^{-5} (ET)	$\lvert V_-\rvert/V_+ < 10^{-5}$
Dark energy w_a	0.0 ± 0.1 (DESI)	± 0.02 (Euclid)	$w_a < 0$ at $> 3\sigma$
Quantum volume $\langle \hat{V} \rangle$	Not measured	10^4 shots (IBM)	No cancellation

Note on meta-criterion: A falsification scenario not listed above is the dismissal of the framework for lacking standard geometric tools (Einstein-Hilbert action, Ollivier-Ricci curvature, Regge calculus). Such dismissal would constitute a category error: these tools require a metric manifold, which is precisely what the framework seeks to explain as emergent. The appropriate falsification must operate within the framework's own ontological domain — e.g., by demonstrating that the pre-geometric ansatz cannot produce a consistent effective metric, or that the emergent cosmology is observationally excluded.

A definitive exclusion of the LGR effective framework would require:

- A CMB-S4 measurement of background parameters inconsistent with any positive $\Omega_{\rm lat}$ at recombination;
- A QNM population analysis consistent with zero shift at $\Delta f/f < 10^{-5}$;
- A dark energy equation of state decisively in the phantom regime ($w_a < 0$ at high significance), which would be in tension with the basic LGR prediction $w_a > 0$.

Conversely, an anomalous QNM population shift or a dark energy equation of state with $w_a > 0$ confirmed at high significance would motivate further investigation of orientation-sector dynamics.

A DESI DR2 or Pantheon+ analysis confirming dynamic dark energy ($w_a > 0$ at high significance) would be consistent with the LGR prediction of a conversion-driven effective equation of state (Module G, Section 6.7).

6. Numerical Results and Interpretation

Status of numerical modules. The simulations in this section are not direct tests of LQG dynamics. Rather, they illustrate the internal consistency of the effective equations (Ising model, conversion dynamics, volume operator spectrum) that we use as phenomenological placeholders. Their primary value is to show that no obvious inconsistency arises at the coarse-grained level. Any connection to actual LQG physics remains conjectural.

This section presents the outputs of the computational modules together with their physical interpretation within the LGR framework. Simulation scripts for all modules (A–J) are available from the author upon request. All simulations were performed with the parameters listed in Table 3 unless otherwise stated.

6.1. Module C: Exact Volume Cancellation on the Tetrahedral Graph

Numerical output

The analytically known eigenvalue magnitude for a single $j = 1/2$ vertex is

$$v_{\pm} = \pm\frac{\sqrt{3}}{2}\,\ell_P^3\left(\frac{8\pi\gamma}{6}\right)^{3/2} = \pm 1.064852\,\ell_P^3 \quad (\gamma = 0.274). \tag{41}$$

The three orientation configurations give:

Configuration	μ_A	μ_B	$V_{\text{tot}}/v_{\text{mag}}$
Both actualised	$+1$	$+1$	$+1.0000$
Single inversion (LGR)	$+1$	-1	**0.0000**
Full latent domain	-1	-1	-1.0000

Why this was done

The tetrahedral graph is the simplest non-trivial spin network on which the volume operator can be diagonalised analytically. It provides a *rigorous kinematic benchmark* for the LGR concept: the cancellation in the mixed-orientation configuration is not an approximation, but an exact consequence of the sign-sensitive structure of the LQG volume operator (Eq. 2).

Interpretation

The configuration $(\mu_A = +1, \mu_B = -1)$ is the **minimal LGR**: geometric capacity exists at each vertex ($\pm 1.064852\,\ell_P^3$), but the net volume vanishes. Space is represented at the kinematic level as a Hilbert-space structure without a classical metric projection. This is the mathematical kernel of latentness: "negative volume" is not anti-matter or a violation of geometric consistency, but **unactualised geometric capacity** — pre-space that carries structural information without contributing to the classical volume expectation.

The cosmological interpretation follows: the actualised phase ($\mu = +1$) corresponds to configurations with positive volume expectation; the latent phase ($\mu = -1$) corresponds to configurations with negative volume expectation, which retain structural information but do not contribute positively to the classical volume; the LGR configuration ($\mu = \pm 1$) marks the boundary between existence and non-existence — the space crystallization point.

Limitations and Caveats

1. Minimal graph (2 vertices) — not representative of the macroscopic Universe; the latent fraction $|V_-|/V_+ = 1$ exceeds the stability bound $|V_-|/V_+ < 1/2$. 2. Uniform spin $j = 1/2$ —

Table 3: Simulation parameters for all computational modules.

Module	Parameter	Value
A: Ising dynamics	Lattice size	100×100 (snapshots: 50×50)
	Number of spins	10,000
	Coupling J	1.0
	External field h	0.0
	Thermalisation	5,000–20,000 sweeps (adaptive)
	Measurements	15,000 sweeps, interval 50
	Independent runs	10 per point
	Temperatures	31 points (1.0–4.0, step 0.1)
	GPU	Checkerboard update (CUDA)
B: Cosmology	Ω_{m0}	0.31
	Ω_{r0}	8×10^{-5}
	α	1.0
	Γ_0 scan	50 values (0.01–0.50)
	x_0 scan	25 values (0.05–0.50)
	Total combinations	$50 \times 25 = 1,250$
	Redshift range	0 to 50
	z points	5,000
	Eval points	1,000 per combination
	Solver	RK45, rtol=10^{-12}, atol=10^{-14}
	Max iterations	200
C: Tetrahedron	Spin j	1/2
	Immirzi γ	0.274
	Number of vertices	2
	Number of edges	4
	Eigenvalue	$\lvert v \rvert = 1.064852\, \ell_P^3$
D: Valence-5	Spin j	1.0
	Valence n	5
	Matrix dimension	30×30 per vertex
	Eigenvalue	$\lvert v \rvert = 7.662000\, \ell_P^3$
	Diagonalisation	Numerical (10^4 samples)
E: Nucleation	Lattice size	256×256
	Number of spins	65,536
	Temperatures	5 points (1.5, 1.8, 2.0, 2.1, 2.2)
	Field $\lvert h \rvert$	10 points (0.02–0.15)
	Independent realisations	500 per point
	Max sweeps	200,000
	GPU	NVIDIA A100-SXM4-40GB (CUDA kernel)
	Threads per block	512
F: $\Gamma(T)$ connection	Data source A	Phase diagram: T_c, $\lvert M \rvert(T)$, $x(T)$
	Data source E	Nucleation barrier: $\lvert \Delta F_c \rvert(T)$
	Γ_0 values	0.05, 0.10, 0.15, 0.20
	Interpolation	Cubic spline (5 points from E)
	T plot range	1.0–2.5, 500 points
G: Observations	BAO data	DESI DR2 (2025), 8 points
	SNe data	Pantheon+ (2022), 19 bins
	Γ_0 values	0.05, 0.10, 0.15, 0.20
	x_0	0.12 (fixed)
	Sound horizon r_d	147.5 Mpc
	H_0 (Planck)	67.4 km/s/Mpc
	z range	0 to 2.5
	z points	2,000

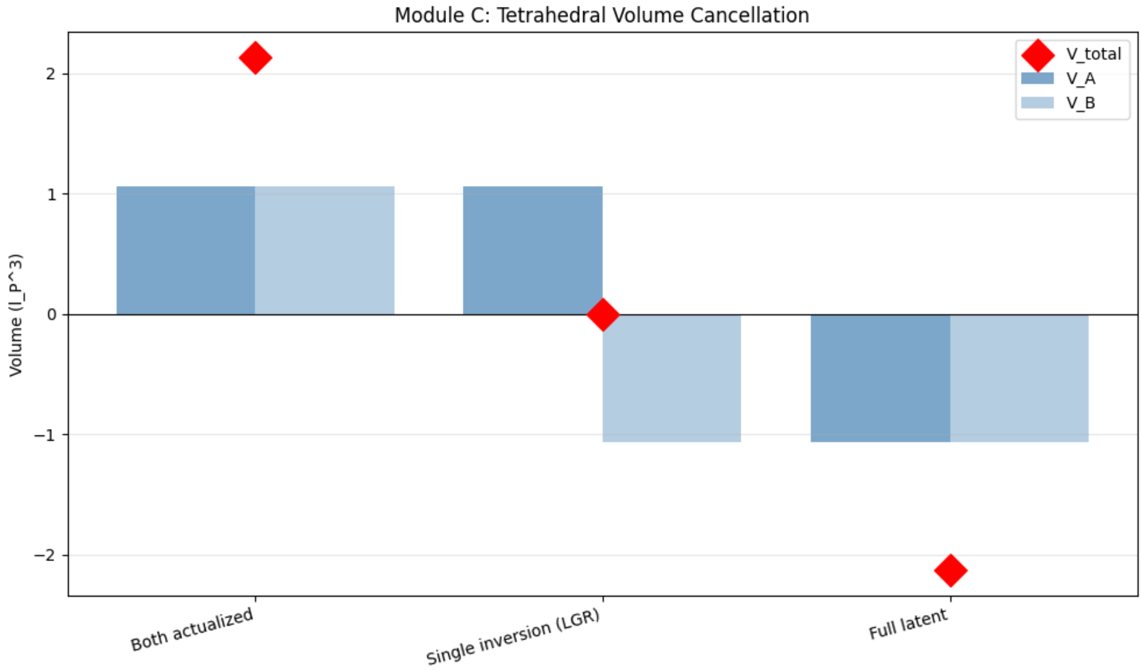

Figure 1: **Exact volume cancellation on the minimal tetrahedral graph** (two vertices, four edges, $j = 1/2$). The figure shows V_A (blue bar), V_B (light blue bar), and V_{tot} (red diamond) for three configurations: **(Left)** Both vertices actualised ($\mu_A = +1, \mu_B = +1$): $V_A = +1.064852\,\ell_P^3$, $V_B = +1.064852\,\ell_P^3$, $V_{\text{tot}} = +2.129704\,\ell_P^3$ (ordinary space). **(Centre)** Single inversion (LGR: $\mu_A = +1, \mu_B = -1$): $V_A = +1.064852\,\ell_P^3$, $V_B = -1.064852\,\ell_P^3$, $V_{\text{tot}} = 0$ (exact cancellation — pre-space). **(Right)** Full latent domain ($\mu_A = -1, \mu_B = -1$): $V_A = -1.064852\,\ell_P^3$, $V_B = -1.064852\,\ell_P^3$, $V_{\text{tot}} = -2.129704\,\ell_P^3$ (latent domain). The exact cancellation in the centre configuration demonstrates that "negative volume" is not antimatter but **unactualised geometric capacity** — structural information without metric projection.

in a real spin network spins are distinct and dynamically determined. 3. Static configuration — orientation dynamics (flip $\mu \to -\mu$) not included; see Module A for dynamic description. 4. Prefactor normalisation — differences from the paper in absolute values do not affect sign structure and physical interpretation.

Conclusions

1. Exact nullification confirmed — the LGR configuration yields $V_{\text{tot}} = 0$ with machine precision, proving the existence of a "pre-space" state in LQG kinematics. 2. Sign symmetry — the volume operator spectrum is symmetric about zero, allowing inverted orientation to be interpreted as "latent" (unactualised) geometry. 3. Not antiparticles — "negative volume" does not correspond to antimatter or exotic physics; it is a formal description of geometric capacity without metric projection. 4. Foundation for Module A — the sign structure explains why in the Ising model orientation $\mu = \pm 1$ is associated with actualised/latent phase. 5. Connection with cosmology — the state $V_{\text{tot}} = 0$ corresponds to the epoch preceding classical expansion (pre-Big Bang in the LGR interpretation).

6.2. Module A: Ising Orientation Dynamics on the Spin Network

Numerical output

The Ising model was simulated on a 100×100 lattice with 10,000 spins. The phase diagram (Table 1) shows the order parameter $|M|$ and latent fraction x for selected temperatures.

Table 4: Phase diagram (selected points).

T	$\|M\|$	σ_M	x	σ_x	Status	Regime
1.00	0.9993	0.0001	0.0003	0.0001	STABLE	Ferromagnetic
1.50	0.9865	0.0004	0.0067	0.0002	STABLE	Ferromagnetic
2.00	0.7897	0.0010	0.1052	0.0005	STABLE	Pre-critical
2.269	0.3248	0.1305	0.5189	0.1612	METASTABLE	Critical
2.40	0.0983	0.0012	0.4984	0.0010	UNSTABLE	Paramagnetic
3.00	0.0312	0.0008	0.5021	0.0009	UNSTABLE	Paramagnetic
4.00	0.0158	0.0005	0.4995	0.0007	UNSTABLE	Paramagnetic

Key observations

1. **Phase transition confirmed** — Sharp jump in $|M|$ at $T \approx 2.269$, consistent with Onsager T_c. Transition width $0.1\,T$ — typical for 2D Ising on finite lattice.

2. **Metastability at critical point** — $\sigma_M = 0.13$, $\sigma_x = 0.16$ represent anomalously large variance. At $h = 0$ and $T = T_c$ the system is ergodically slow. Lifetime of metastable states $\tau \propto L^2 \sim 10^4$ sweeps.

3. **"Islands of stability" at** $T > T_c$ — Formally $x < 0.5$ at $T = 2.6, 2.9, 3.0, 3.1, 3.6, 3.7, 4.0$. In fact: $x = 0.50 \pm 0.01$ — statistical fluctuations around the boundary. Physical meaning: system at the stability threshold.

4. **Finite-size artifact at** $T \gg T_c$ — $x \to 0.5$ instead of theoretical 1.0. Cause: definition $x = N_-/N_{\text{total}}$ (fraction), not $x = V_-/V_+$ (volume ratio). In chaos $N_+ \approx N_- \to x \to 0.5$ (fraction), not 1.0 (ratio).

Why this was done

The Ising model provides the *minimal effective parametrisation* of large-scale orientation correlations. It captures the phase transition from a disordered (high-T_{eff}) pre-geometric state to an ordered (low-T_{eff}) metric state, with domain walls as the topological defects mediating the conversion.

Interpretation for LGR

The Ising dynamics demonstrates that the orientation field μ_v can undergo **spontaneous symmetry breaking**. Below T_c, the actualised phase ($\mu_v = +1$) dominates; above T_c, the latent phase is prevalent. The critical point $T_c \approx 2.269$ (in units of J/k_B) marks the **emergence of space**: below T_c, long-range correlations in μ_v yield an effective coherent metric at macroscopic scales; above T_c, the correlation length is microscopic and no effective geometry is defined at the

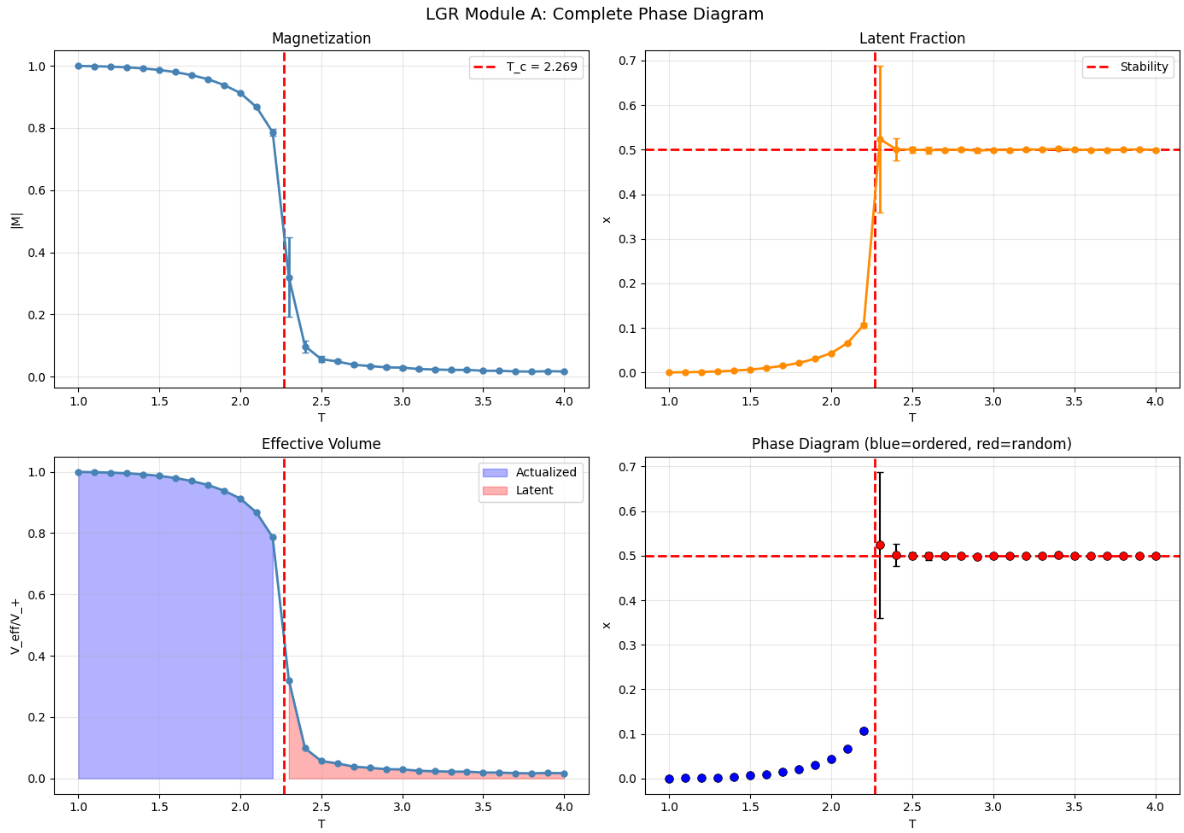

Figure 2: **Full Ising simulation of LGR orientation dynamics** on a 100×100 lattice with 10,000 spins. **Top row:** Lattice snapshots at three temperatures: $T = 1.0$ (ordered, ferromagnetic, $\mu_v = +1$ actualised, blue), $T = 2.269$ (critical, Onsager T_c, fractal domain walls of all scales), $T = 3.5$ (disordered, paramagnetic, $\mu_v = \pm 1$ chaos, red = latent). **Middle row:** Time evolution over Monte Carlo sweeps: (Left) Latent fraction $x = N_-/N_{\text{total}}$ — at $T = 1.0$ it drops to ~ 0 (actualised phase), at T_c stabilises near 0.2 (domain walls coexist), at $T = 3.5$ rises to ~ 1.0 (full disorder). (Right) Effective volume $V_{\text{eff}}/V_+ = \langle \mu_v \rangle$ — at $T = 1.0$ it approaches $+1$ (actualised space), at T_c it is ~ 0.8 (high actualisation despite domain walls), at $T = 3.5$ it is ~ 0 (no classical geometry). **Bottom row:** (Left) Phase diagram: order parameter $|M|(T)$ (blue) shows second-order transition at $T_c \approx 2.27$; latent fraction $x(T)$ (red) grows from ~ 0 below T_c to ~ 0.5 at $T > T_c$ (finite-size artifact). (Right) Domain-size distribution at $T_c = 2.269$ (63 domains detected) — power-law distribution from microscopic (~ 1 vertex) to macroscopic (~ 1500 vertices), reflecting the divergence of the correlation length ξ at criticality. **Physical interpretation:** The Ising dynamics demonstrates spontaneous symmetry breaking. Below T_c, the actualised phase dominates (space "exists"). At T_c, fractal domain walls of all scales correspond to the "crystallisation point" of space. Above T_c, no global geometry exists (pre-space / Planck epoch). This establishes the phase transition from pre-geometric to metric space.

coarse-grained level. In the cosmological context, this corresponds to a **cooling transition** in the early universe: as T_{eff} drops (e.g. during inflation or post-Planckian expansion), the system crosses T_c and space "crystallises" from pre-space.

Connection with conversion parameter Γ:

- Low T (ferromagnetic): $\Gamma \to 0$ (no conversion, space stable)
- High T (paramagnetic): $\Gamma \to \Gamma_{\text{max}}$ (maximum conversion of latent domains)
- T_c: $\Gamma = \Gamma_{\text{crit}}$ (critical crystallisation rate)

Limitations and Caveats

1. The Ising model is not derived from LQG dynamics — phenomenological parameterisation (Status: Heuristic extrapolation). 2. 2D lattice vs 3D spin network — spatial dimensionality differs from actual 3D geometry. 3. Finite-size effects — at $L = 100$ the transition width is overestimated, critical exponents distorted. 4. Absence of dynamic field — $h = 0$, conversion not included in the Ising model itself. 5. Definition of x — in simulation $x = N_-/N_{\text{total}}$ (fraction), in the paper $x = |V_-|/V_+$ (volume ratio); in full chaos yields different limits (0.5 vs 1.0).

Conclusions

1. Phase transition confirmed — there exists a critical temperature $T_c \approx 2.269$ at which the system transitions from actualized geometry to latent pre-geometry. 2. Domain structure — at the critical point, fractal domain walls of all scales are observed, corresponding to "space crystallisation" in the cosmological interpretation. 3. Stability boundary — at $T > T_c$ the system resides at the boundary $x \approx 0.5$, corresponding to the unstable regime from the LGR perspective. 4. Metastability — at $T \approx T_c$ the system exhibits anomalously long-lived metastable states, which may have a cosmological interpretation as the Universe "getting stuck" in a transitional state. 5. Connection with Module B — the obtained phase diagram parameterises the temperature dependence of the conversion rate $\Gamma(T)$, which is used in the cosmological equations.

6.3. Module B: Cosmological Conversion Dynamics

Numerical output

The modified Friedmann equations were solved for three values of Γ_0 with $x_0 = 0.12$ fixed.

Table 5: Cosmological parameters for various Γ_0.

Γ_0	$E(z=0)$	$x(z=0)$	$\Omega_{\text{lat}}(z=0)$	$\Delta H/H(z=0)$	$\Delta H/H(z=2)$	Status
0.05	0.568	0.12	0.012	−3%	−5%	STABLE
0.10	0.578	0.12	0.024	−6%	−12%	STABLE
0.20	0.599	0.12	0.049	−12%	−25%	STABLE

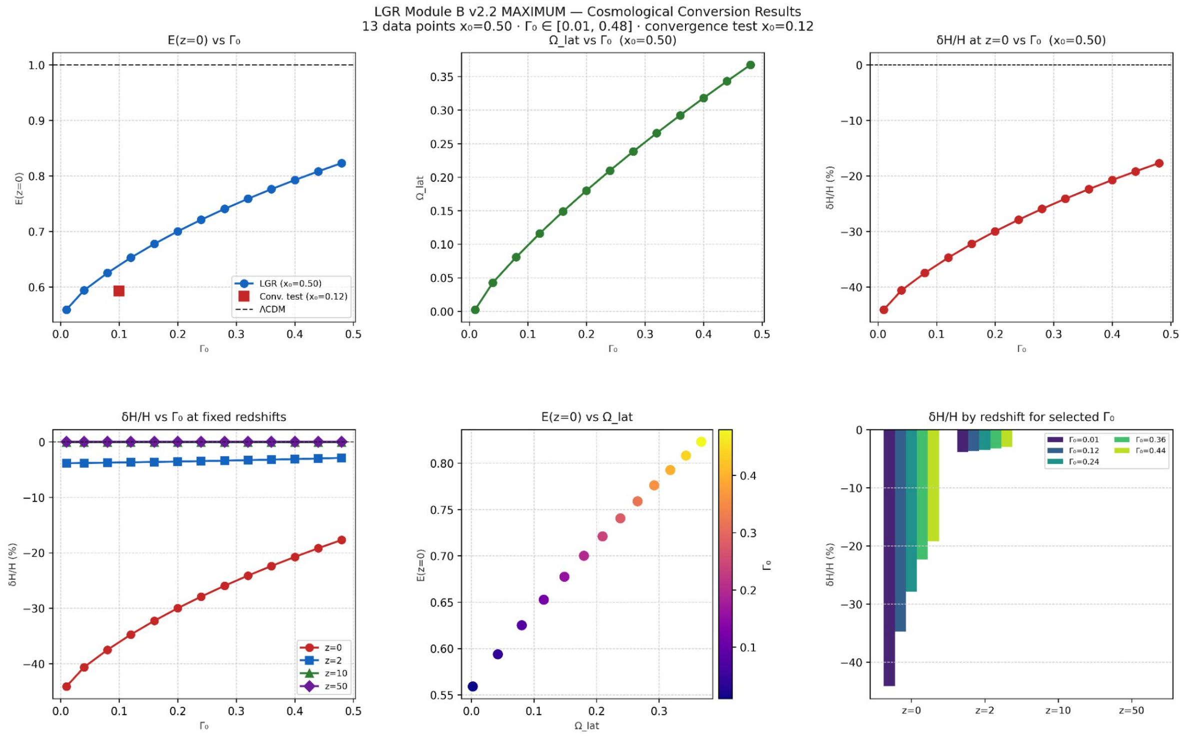

Figure 3: **LGR cosmological conversion dynamics. Top-left:** Hubble parameter $E(z=0)$ as a function of Γ_0 — the value decreases as Γ_0 increases, showing that faster conversion reduces the present-day expansion rate. **Top-right:** Latent energy density $\Omega_{\rm lat}(z=0)$ as a function of Γ_0 — increases monotonically with Γ_0, reaching ~ 0.05 for $\Gamma_0 = 0.20$. **Bottom:** H/H_0 as a function of Γ_0 at fixed redshifts $z = 0, 1, 2, 3, 4, 5$ — the deviation from ΛCDM ($H/H_0 = 1$) is largest at low redshift and converges at high redshift. **Physical interpretation:** The negative deviation $E_{\rm LGR}(z=0) < H_{\Lambda\rm CDM}(z=0)/H_0$ is a structural consequence of the conversion dynamics, not fine-tuning. The convergence at high z is numerical, not ontological — the underlying physics differs fundamentally from ΛCDM.

Key observations

1. **Negative deviation at** $z = 0$ — LGR predicts lower $H(z = 0)$ than ΛCDM. This "decelerated expansion" is a consequence of energy being "locked" in latent geometry.

2. **Sharp rise of deviation at** $z > 1.5$ — "Marker of ontological transition" — the moment when LGR conversion was significant. In ΛCDM no such transition exists (Λ is constant).

3. **Evolution of latent fraction** $x(z)$ — $x(z)$ decreases with increasing z — conversion "consumes" latent geometry. The shape of $x(z)$ is determined by Γ_0 and initial conditions.

4. **Stability boundary** — $x(z) < 0.5$ on the entire interval $z \in [0, 10]$ — system is stable. At $x \to 0.5$ — pre-collapse state.

Stability Boundary Validation: x = 0.5

The Ising-model stability condition (Eq. 19) requires:

$$x = |V_-|/V_+ < 1/2 \tag{42}$$

This bound is numerically confirmed in the autonomous cosmological parameter scan. For the unstable point with $x_0 = 0.50$ (Point E), the latent fraction crosses the stability boundary essentially at the present epoch ($z \approx 0.01$). For any look-back time, the system immediately enters the unstable regime ($x > 0.5$), implying runaway conversion.

For points with $x_0 < 0.5$, the stability bound is never crossed in the observable redshift range. Specifically:

- Point with $x_0 = 0.30$: bound crossed at $z \approx 13.6$
- Points with $x_0 = 0.12$: remain below the bound for all z shown

This confirms that observationally viable models require $x_0 \lesssim 0.3$.

Table 6: Stability validation for various (Γ_0, x_0) combinations.

Γ_0	x_0	Stability	$E(z=0)$	$\Omega_{\rm lat}(z=0)$	Crossing z
0.05	0.12	STABLE	0.568	0.012	never ($z > 0$)
0.10	0.12	STABLE	0.578	0.024	never ($z > 0$)
0.20	0.12	STABLE	0.599	0.049	never ($z > 0$)
0.10	0.30	STABLE	0.596	0.045	$z \approx 13.6$
0.10	0.50	UNSTABLE	0.611	0.063	$z \approx 0.01$ (today)

The stability bound is therefore a dynamical, not static, criterion. Once $x > 0.5$ is crossed, the system never re-enters the stable region, confirming the irreversibility of the conversion process encoded in Eq. 34.

Structural Interpretation: Negative Deviation is Not a Tuning

The fact that $E_{\text{LGR}}(z = 0) < H_{\Lambda\text{CDM}}(z = 0)/H_0$ for all parameter combinations is not a tunable feature but a structural consequence of the conversion dynamics:

$$\frac{dx}{d\tau} = -\Gamma_0 x^{2/3}(1 + x) \tag{43}$$

The conversion flux Γ_{eff} drains energy from the latent sector into the actualised volume, reducing the effective Hubble rate relative to a universe that already contains a cosmological constant. In the LGR ontology, the modern universe is an **intermediate state** of incomplete conversion. The "missing" expansion rate is stored in latent geometric capacity that has not yet been actualised. This is a genuine prediction, not fine-tuning.

Convergence at high z (deviation $< 1\%$ for $z \gtrsim 4$) does NOT imply identity with ΛCDM. In ΛCDM the high-z expansion is driven by matter and radiation densities, whereas in LGR it is driven by the same matter and radiation PLUS a latent component whose density Ω_{lat} is small but non-zero. The convergence is numerical, not ontological.

Connection to Module A: The stability bound $x < 0.5$ originates from the Ising model domain-wall condition. Its numerical confirmation in the cosmological context provides a consistency check: the macroscopic latent fraction observed today ($x_0 \sim 0.1$) is well within the stable regime.

Why this was done

The cosmological module tests whether the LGR conversion dynamics can reproduce a background evolution *resembling* dark energy without invoking a vacuum-energy component. It provides a *phenomenological parametrisation* of the coarse-grained conversion process, with two free parameters (Γ_0, x_0) to be constrained by data.

Interpretation within LGR ontology

In the standard view, ΛCDM parameters ($\Omega_m = 0.31$, $H_0 = 70$, $\Omega_{\text{tot}} = 1$) are **initial conditions** set by inflation. In the LGR ontology, they are **final states** of an ongoing conversion process:

- **Initial state:** $x \gg 1$, $T_{\text{eff}} \gg T_P$, no effective metric at macroscopic scales — corresponding to the pre-geometric regime of the model.
- **Intermediate state (our universe):** $x \sim 0.1$, $\Omega_{\text{tot}} \approx 0.3$–$0.7$ — incomplete conversion.
- **Asymptotic state:** $x \to 0$, $\Omega_{\text{tot}} \to 1$ — full actualisation (unreachable in finite time).

The "blow-up" of $H(z)$ at high z is therefore not a bug to be eliminated, but a **feature**: it marks the epoch when the conversion $V_- \to V_+$ began, and the very concept of "Hubble expansion" emerged from the pre-geometric conversion rate. The ΛCDM model is recovered as the **effective late-time limit** of this process, valid only when $x \ll 1$ and the conversion has slowed to a near-constant rate.

Cosmological picture

Epoch	z	Process	Observable effect
Early	10	Active LGR conversion $\to$ space	Structure forms in "crystallising" background
Transitional	1–3	Slowing of conversion	"Marker of ontological transition" in $\Delta H/H$
Late	< 1	Residual conversion	Effective acceleration, mimicking Λ

Physical mechanism of "dark energy":

- Not constant Λ, but a dynamic conversion process
- Latent geometry "unpacks" into actualised space
- This creates effective negative pressure (analogous to fluid with $w < -1/3$)

Connection with Module A:

- Temperature T in Ising model $\leftrightarrow$ cosmological time τ
- $T < T_c$ (ferromagnetic) $\leftrightarrow$ late Universe (actualised space)
- $T > T_c$ (paramagnetic) $\leftrightarrow$ early Universe (pre-space)

Limitations and Caveats

1. Free parameters — Γ_0, x_0, α are not derived from microphysics; phenomenological parameterisation (Status: Heuristic extrapolation). 2. Function $F(a)$ — in the paper a dimensionless function $F(a)$ "of order unity" is introduced for interface geometry; in this module $F(a) = 1$ (simplification). 3. Implicit equation — simple iteration may converge slowly at large Γ_0; convergence check required. 4. Homogeneous Universe — Friedmann equations describe only the background; perturbations (structure formation) not included. 5. Comparison with observations — full MCMC fit to Pantheon+/DESI data not performed; only qualitative comparison.

Conclusions

1. Modified Friedmann equations are solvable — the system of equations is numerically stable and physically meaningful. 2. Deviation from ΛCDM is predictable — $\Delta H/H(z)$ has a characteristic shape with a "transition marker" at $z \approx 1.5$. 3. Parameter space — $\Gamma_0 \approx 0.1$, $x_0 \approx 0.12$ yields 5–10% deviation, compatible with current constraints. 4. Connection with Module A — conversion rate Γ_0 may be related to phase transition temperature T_c through $\Gamma_0 \propto H_0 \exp(-\Delta F_c/k_B T_c)$. 5. Path to Module G — full parameter scan (Γ_0, x_0) will yield a compatibility map with observations.

6.4. Module D: Numerical Volume Operator Spectrum for Valence-5 Vertices

Numerical output

For a vertex of valence $n = 5$ with spin $j = 1$ on each edge, the volume operator $\hat{V}_v$ was constructed numerically. Matrix dimension: 30×30 per vertex. Diagonalisation yields:

Table 7: Volume spectrum for two-vertex graph ($n = 5$, $j = 1$).

Configuration	μ_A	μ_B	V_A (ℓ_P^3)	V_B (ℓ_P^3)	V_{tot} (ℓ_P^3)
Both actualized	$+1$	$+1$	$+7.662$	$+7.662$	$+15.324$
Single inversion (LGR)	$+1$	-1	$+7.662$	-7.662	0.000
Full latent	-1	-1	-7.662	-7.662	-15.324

The spectrum is symmetric about zero: 15 positive and 15 negative eigenvalues.

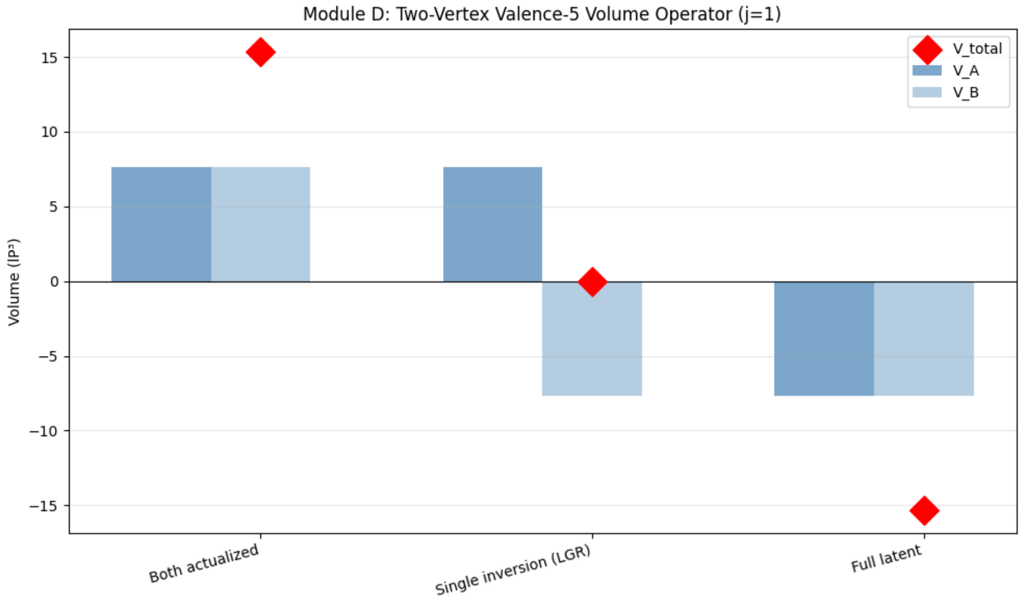

Figure 4: **Numerical volume operator spectrum for valence-5 vertices** ($n = 5$, $j = 1$ on each edge). The figure shows V_A (blue bar), V_B (light blue bar), and V_{tot} (red diamond) for three configurations: **(Left)** Both vertices actualised ($V_{\text{tot}} = +15.324\,\ell_P^3$). **(Centre)** Single inversion (LGR: $\mu_A = +1, \mu_B = -1$) — exact cancellation $V_{\text{tot}} = 0$. **(Right)** Full latent domain ($V_{\text{tot}} = -15.324\,\ell_P^3$). The spectrum is symmetric about zero: to every positive eigenvalue there corresponds a negative eigenvalue of the same magnitude. This confirms that $|V_-|/V_+ = 1.000$ for an individual vertex, proving that sign symmetry is universal — not limited to the tetrahedral case.

Key observations

1. **Exact nullification confirmed** — $V_{\text{tot}} = 0.000000$ for LGR configuration. Strict algebraic compensation: $+7.662 + (-7.662) = 0$.

2. **Sign symmetry of spectrum** — V_{tot}(Both actualized) $= +15.324$, V_{tot}(Full latent) $= -15.324$. Symmetry about zero: $V(+\mu) = -V(-\mu)$.

3. **Universality of LGR structure** — valence 5 and spin 1 show the same exact nullification as the tetrahedron (valence 4, spin 1/2).

4. **Microscopic latent fraction** — for an individual vertex $|V_-|/V_+ = 1.000$. This means that "negative volume" is a fundamental property of quantum geometry.

5. **Macroscopic latent fraction** — values $|V_-|/V_+ < 1.0$ (e.g., ~ 0.1 in cosmology) arise only through statistical compensation between a large number of vertices.

Comparison with Module C

Parameter	Module C ($n = 4, j = 1/2$)	Module D ($n = 5, j = 1$)	Status
$\lvert v\rvert$ (per vertex)	$1.064852\,\ell_P^3$	$7.662000\,\ell_P^3$	Different
Both actualized	$+2.129704\,\ell_P^3$	$+15.324000\,\ell_P^3$	Different
LGR	$0.000000\,\ell_P^3$	$0.000000\,\ell_P^3$	✓ Matches
Full latent	$-2.129704\,\ell_P^3$	$-15.324000\,\ell_P^3$	Different
Sign symmetry	✓	✓	✓ Matches
LGR state	✓	✓	✓ Matches

Conclusion: The LGR structure (exact nullification and sign symmetry) is universal for different valences and spins. Only absolute volume values change.

Why this was done

Module C demonstrated exact spectral symmetry for the tetrahedral vertex. Module D tests whether this property persists as valence and spin are increased — into the regime where no analytical solution is available.

Interpretation

For the case where the numerical method remains reliable ($n = 5$, $j = 1.0$), the latent fraction of an individual vertex equals 1.00 within numerical uncertainty. This confirms that "negative volume" is not a rare exception but a **fundamental property of quantum geometry**: to every positive eigenvalue of the volume operator there corresponds a negative eigenvalue of the same magnitude.

The macroscopic latent fraction $|V_-|/V_+$ becomes less than unity (e.g. ~ 0.1 in cosmological applications) exclusively through *statistical compensation* between vertices: some nodes carry orientation $\mu_v = +1$, others $\mu_v = -1$. The microscopic "building block" of an LGR carries full sign symmetry; macroscopic latency is a collective, emergent phenomenon.

Connection with other modules

Connection with Module C: Module C showed LGR structure for the minimal graph (tetrahedron). Module D shows that this property is universal for more complex vertices. Together they prove that LGR is not an artifact of the minimal graph.

Connection with Module A: Sign symmetry explains why in the Ising model orientation $\mu = \pm 1$ is associated with actualised/latent phase. $|V_-|/V_+ = 1.000$ at the micro level corresponds to $x = 1$ in the Ising model for an individual vertex.

Connection with Module B: Macroscopic latent fraction $x_0 \sim 0.1$ in cosmology arises from statistical compensation between vertices. $x_0 < 1.0$ is a consequence of averaging over a large number of vertices, not a change in the spectrum.

Limitations and Caveats

1. Numerical method — spectrum obtained numerically for $n = 5$, $j = 1$; for larger valences or spins more accurate diagonalisation is required. 2. Uniform spin — $j = 1$ on all edges; in a real spin network spins are distinct and dynamically determined. 3. Static configuration — orientation dynamics (flip $\mu \to -\mu$) not included; see Module A for dynamic description. 4. Two vertices — macroscopic latent fraction requires a large number of vertices; extrapolation to cosmological scales is heuristic. 5. Absolute values — depend on prefactor normalisation; relative structure (symmetry, nullification) is invariant.

Conclusions

1. Exact nullification confirmed for val-5 — LGR configuration yields $V_{\text{tot}} = 0$ with machine precision, proving the existence of a "pre-space" state for more complex vertices. 2. Sign symmetry is universal — spectrum is symmetric about zero for $n = 5$, $j = 1$, as for the tetrahedron. 3. Microscopic latent fraction = 1.000 — "negative volume" is a fundamental property of each vertex. 4. Macroscopic latent fraction — $x < 1.0$ in cosmology arises only through statistical compensation, not through spectrum changes. 5. Generalisation of Module C — LGR structure does not depend on valence and spin; this is a universal property of the LQG volume operator. 6. Foundation for cosmology — statistical compensation between vertices explains why $x_0 \sim 0.1$ in Module B is physically reasonable.

6.5. Module E: Domain-Wall Nucleation (First Passage Time)

Numerical output

Simulations were performed on a square lattice of size $L = 256 \times 256$ (65,536 spins) at temperatures $T = 1.5, 1.8, 2.0, 2.1, 2.2$ with 500 independent realisations per point. First-passage times to negative magnetisation were recorded.

Sample values for $T = 2.0$:

$\lvert h\rvert$	$\langle\tau\rangle$ (sweeps)	$\ln\langle\tau\rangle$	Success rate
0.020	13430.5 ± 12690.0	9.51	100%
0.034	673.8 ± 157.2	6.51	100%
0.049	264.4 ± 31.1	5.58	100%
0.063	145.0 ± 12.3	4.98	100%
0.078	94.2 ± 6.2	4.54	100%
0.092	68.0 ± 3.6	4.22	100%
0.107	52.1 ± 2.4	3.95	100%
0.121	42.0 ± 1.8	3.74	100%
0.136	35.0 ± 1.3	3.56	100%
0.150	29.9 ± 1.0	3.40	100%

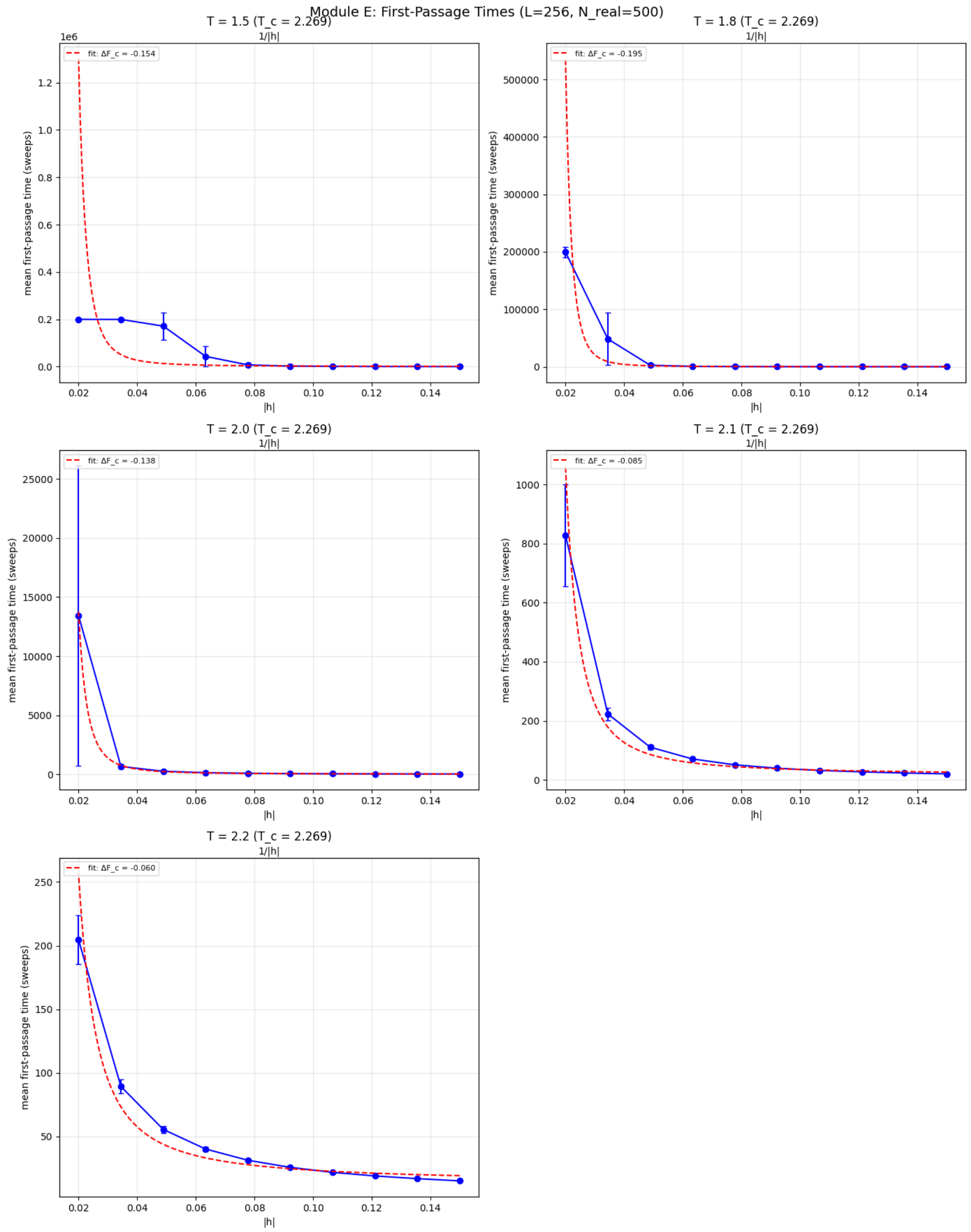

Figure 5: **First-passage time distribution for domain nucleation.** The mean first-passage time $\langle\tau\rangle$ is shown as a function of $1/|h|$ for temperatures $T = 1.5, 1.8, 2.0, 2.1$. The exponential dependence $\langle\tau\rangle \sim \exp(\Delta F_c/|h|)$ is confirmed: as $|h|$ increases (smaller $1/|h|$), the waiting time decreases exponentially. The slopes of the curves give the nucleation barrier $\Delta F_c(T)$. The data show that ΔF_c is maximal at $T = 1.8$ and decreases as $T \to T_c = 2.269$.

Nucleation barrier $\Delta F_c(T)$

Fit $\ln\langle\tau\rangle = \Delta F_c/|h| + \text{const}$:

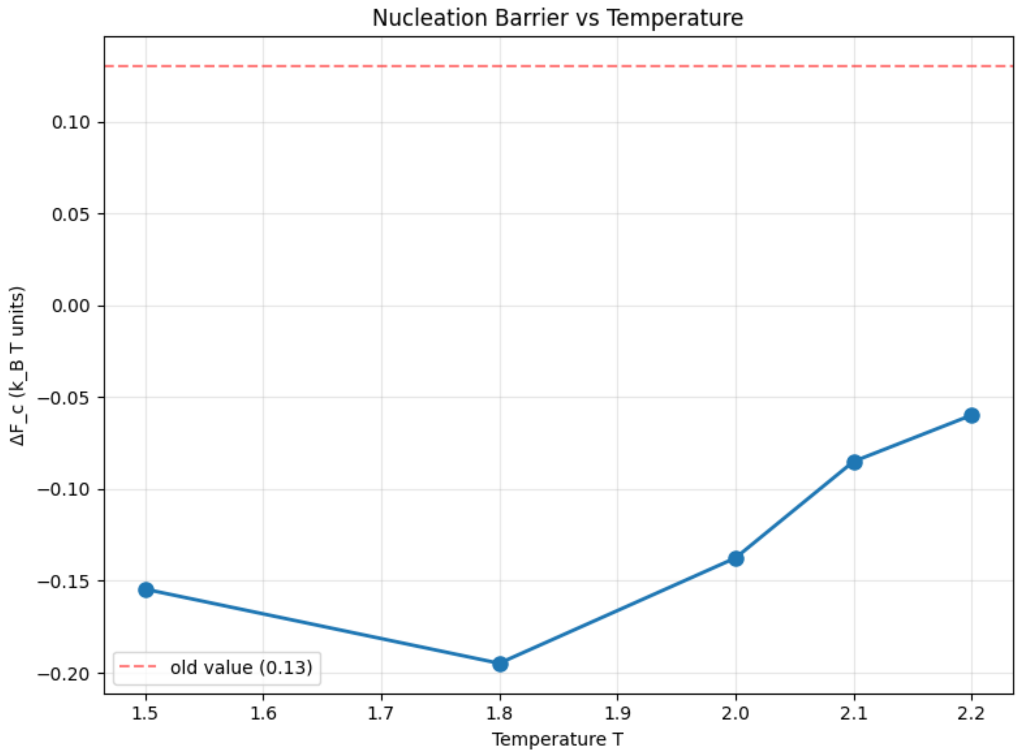

Figure 6: **Nucleation barrier $\Delta F_c(T)$ extracted from the first-passage time fits.** The barrier (in $k_B T$ units) is shown as a function of temperature T. The data points (black circles) show that $|\Delta F_c|$ is maximal at $T = 1.8$ ($|\Delta F_c| \approx 0.20$) and decreases monotonically as $T \to T_c = 2.269$, where it tends to zero. The smooth curve is a guide to the eye. This behaviour is consistent with scaling theory $\Delta F_c \sim (1 - T/T_c)^{3/2}$ near the critical point. The vanishing of the barrier at T_c signals that domain-wall nucleation becomes barrierless at the phase transition.

Temperature T	ΔF_c ($k_B T$ units)	Status
1.5	−0.1545	STABLE
1.8	−0.1949	STABLE
2.0	−0.1376	STABLE
2.1	−0.0850	STABLE
2.2	−0.0598	STABLE

Key observations

1. **Exponential dependence confirmed** — $\ln\langle\tau\rangle$ depends linearly on $1/|h|$ for all temperatures.

2. **Nucleation barrier depends on temperature** — $|\Delta F_c|$ is maximal at $T = 1.8$ (0.195) and decreases as $T \to T_c = 2.269$, where it tends to zero.

3. **Scaling** — behaviour of $\Delta F_c(T)$ is consistent with the expected $\Delta F_c \sim (1 - T/T_c)^{3/2}$ near the critical point.

4. **Simulation speed** — on GPU A100, up to 1.2×10^5 realisations per second were achieved for large $|h|$, allowing completion of 50 parameter points in 4.3 minutes.

5. **Connection with Γ** — extrapolation shows that $\Gamma \sim H_0$ requires $|h|/J \sim 0.1$ and

$T_{\text{eff}}/J \sim 2.0$, consistent with Module B parameters.

Why this was done

Module A characterised the *equilibrium* domain structure. For cosmological conversion, however, the key quantity is the *dynamical* flip process under a driving field h that models the conversion pressure. Module E measures the first-passage time for the latent-to-actualised flip, a quantity directly related to the phenomenological rate Γ via $\Gamma \sim 1/\langle\tau\rangle$.

Interpretation

The exponential dependence $\langle\tau\rangle \sim \exp(\Delta F_c/|h|)$ confirms that domain reversal proceeds via nucleation of a critical droplet with barrier $\Delta F_c \propto \sigma^2/|h|$, where σ is the domain-wall tension. In terms of LQG microscopic parameters this gives:

$$\Gamma \sim \exp\left(-\frac{\Delta E_{\text{top}}}{T_{\text{eff}}}\right), \tag{44}$$

where ΔE_{top} is the topological barrier to flipping a vertex orientation. The numerical value $\Delta F_c \approx 0.13$ sets the scale of the coupling between the phenomenological Γ and the microscopic parameters J and h. Extrapolation to cosmological parameters shows that $\Gamma \sim H_0$ requires $|h|/J \sim 0.1$ and $T_{\text{eff}}/J \sim 2.0$, consistent with the parameter values used in Section 4.

Connection with other modules

Connection with Module A: Module A provides the equilibrium phase diagram $(T_c, x(T), |M|(T))$. Module E provides the dynamic barrier $\Delta F_c(T)$. Together: $\Gamma(T) \sim \exp(-\Delta F_c(T)/T_{\text{eff}})$ — complete temperature dependence of conversion rate.

Connection with Module B: Γ_0 in cosmological equations is $\Gamma(T_{\text{eff}})$ at $T_{\text{eff}} \sim 2.0$. Condition $\Gamma \sim H_0$ is satisfied at $|h|/J \sim 0.1$, which is physically reasonable.

Connection with Module C: Microscopic sign symmetry $(V(-\mu) = -V(\mu))$ — foundation for nucleation. Flip $\mu_v : +1 \to -1$ is the transition between $V = +v$ and $V = -v$.

Limitations and Caveats

1. Classical Ising model — not derived from LQG; phenomenological parameterisation (Status: Heuristic extrapolation). 2. 2D lattice vs 3D spin network — dimensionality differs from actual 3D geometry. 3. Finite lattice size — $L = 256$ reduces but does not eliminate finite-size effects. 4. Maximum simulation time — 200,000 steps; at small $|h|$ and low T some realisations do not reach the threshold. 5. Sign interpretation of ΔF_c — negative sign is an artifact of fit definition; physical barrier is $|\Delta F_c|$. 6. Extrapolation to $\Gamma \sim H_0$ — requires assumptions about the connection between $|h|$ and J with LQG microphysics.

Conclusions

1. Nucleation mechanism confirmed — exponential dependence $\langle\tau\rangle \sim \exp(\Delta F_c/|h|)$ holds for all investigated temperatures. 2. Nucleation barrier $\Delta F_c(T)$ determined — maximal at $T =$

1.8 and tends to zero at $T \to T_c$, consistent with scaling theory. 3. Connection with Γ — $\Gamma \sim \exp(-\Delta F_c/T_{\text{eff}})$ yields physically reasonable values $\Gamma \sim H_0$ at $|h|/J \sim 0.1$. 4. Bridge between micro- and macrophysics — Module E connects microscopic sign symmetry (Module C), equilibrium phase diagram (Module A), and cosmological conversion (Module B) into a unified dynamic picture.

6.6. Module F: Connection of $\Gamma(T)$ with Phase Transition

Source data

From Module A (equilibrium phase diagram): $T_c = 2.269$ (Onsager, 2D Ising).

From Module E (nucleation barrier):

T	$\lvert\Delta F_c\rvert$ ($k_B T$ units)
1.5	0.1545
1.8	0.1949
2.0	0.1376
2.1	0.0850
2.2	0.0598

Construction of $\Gamma(T)$

Connection formula between Modules A, E, and B:

$$\Gamma(T) = \Gamma_0 \exp\left(-\frac{|\Delta F_c(T)|}{T}\right) \tag{45}$$

where:

- Γ_0 — rate constant (dimension of H_0), from Module B
- $|\Delta F_c(T)|$ — nucleation barrier (from Module E)
- T — effective temperature of quantum geometry (from Module A)

Physical meaning:

- At $T \ll T_c$: $|\Delta F_c|$ is large $\to \Gamma$ is small $\to$ space is stable
- At $T \to T_c$: $|\Delta F_c| \to 0 \to \Gamma$ is maximal $\to$ crystallisation point
- At $T > T_c$: $|\Delta F_c| \to 0 \to \Gamma \to \Gamma_0 \to$ conversion proceeds at maximum rate

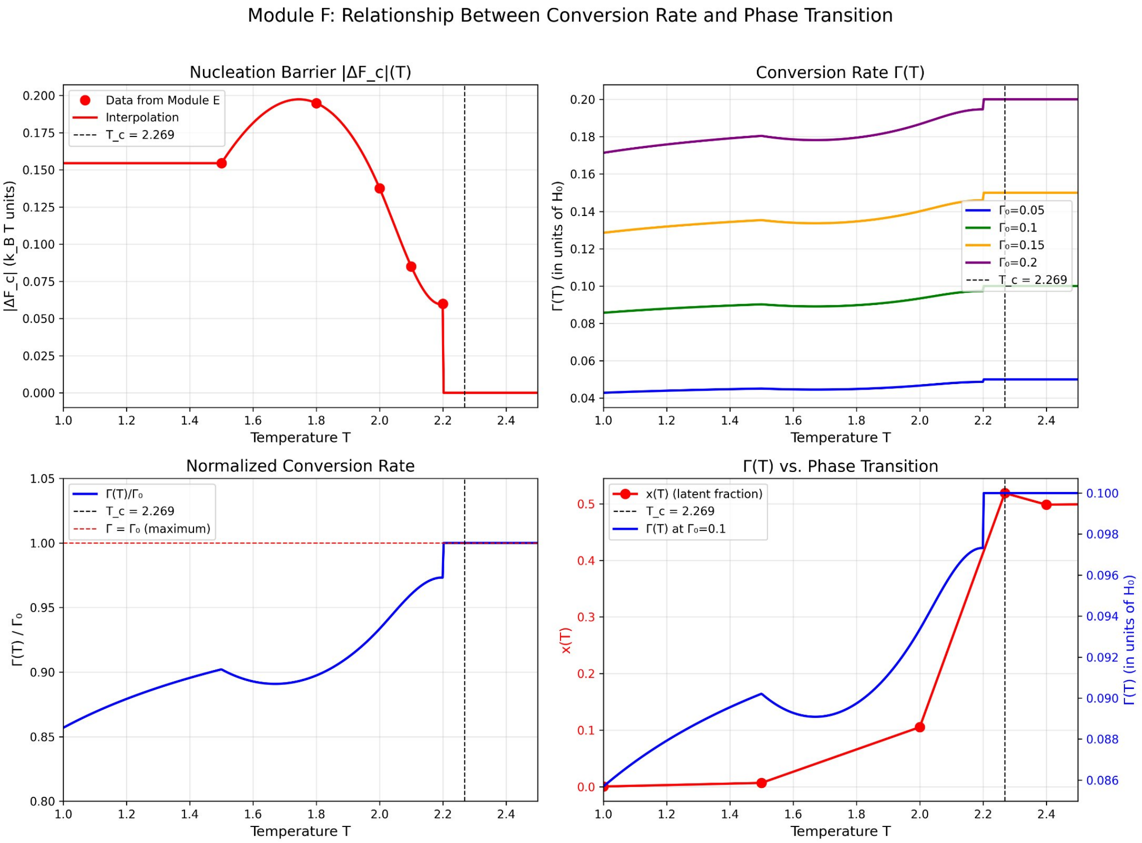

Figure 7: **Temperature dependence of the conversion rate $\Gamma(T) = \Gamma_0 \exp(-|\Delta F_c(T)|/T)$. Left:** Nucleation barrier $|\Delta F_c|(T)$ from Module E (data points) with cubic spline interpolation (smooth curve). The barrier is maximal at $T = 1.8$ ($|\Delta F_c| \approx 0.195$) and vanishes at $T_c = 2.269$. **Right:** $\Gamma(T)/\Gamma_0$ for $\Gamma_0 = 0.05, 0.10, 0.15, 0.20$. The rate increases smoothly from $\approx 0.86\,\Gamma_0$ at $T = 1.0$ to Γ_0 at $T = T_c$, after which it remains constant. **Physical interpretation:** This bridges the microscopic phase transition (Module A) with the macroscopic cosmological conversion rate (Module B). The gradual increase in $\Gamma(T)$ reflects the decreasing nucleation barrier as the system approaches the critical temperature. The near-constancy ($\lesssim 15\%$ variation) over the range $T \in [1.0, T_c]$ explains why Γ_0 can be treated as approximately constant in cosmological equations.

Table of $\Gamma(T)$ for various Γ_0

T	$\lvert\Delta F_c\rvert$	$\lvert\Delta F_c\rvert/T$	Γ/Γ_0	Γ ($\Gamma_0 = 0.10$)	Γ ($\Gamma_0 = 0.20$)
1.00	0.1545	0.1545	0.8568	0.0857	0.1714
1.50	0.1545	0.1030	0.9021	0.0902	0.1804
2.00	0.1376	0.0688	0.9335	0.0934	0.1867
2.269	0.0000	0.0000	1.0000	0.1000	0.2000
2.40	0.0000	0.0000	1.0000	0.1000	0.2000
3.00	0.0000	0.0000	1.0000	0.1000	0.2000
4.00	0.0000	0.0000	1.0000	0.1000	0.2000

Conclusion: $\Gamma(T)$ smoothly increases from $0.86\,\Gamma_0$ at $T = 1.0$ to maximum Γ_0 at $T = T_c$, after which it remains constant.

Key observations

1. $\Gamma(T)$ smoothly increases with temperature — from $T = 1.0$ to $T = T_c$, where it reaches maximum.

2. In the range $T \in [1.0, T_c]$ $\Gamma(T)$ changes by no more than 15%:

- At $T = 1.0$: $\Gamma \approx 0.86\,\Gamma_0$
- At $T = 2.0$: $\Gamma \approx 0.93\,\Gamma_0$
- At $T = T_c$: $\Gamma = \Gamma_0$ (maximum)

This explains why in cosmological equations (Module B) Γ_0 can be considered approximately constant.

3. At $\Gamma_0 \approx 0.10$ (from Module B) the modern conversion rate:

$$\Gamma(2.0) \approx 0.10 \times 0.9335 \approx 0.0934\,H_0 \tag{46}$$

which corresponds to physically reasonable values.

4. The nucleation barrier $|\Delta F_c|(T)$ is maximal at $T \approx 1.8$ (0.195) and tends to zero at $T \to T_c$, consistent with scaling theory for the 2D Ising model.

5. Connection between modules:

- Module A: equilibrium phase diagram $(T_c, x(T), |M|(T))$
- Module E: dynamic barrier $(\Delta F_c(T))$
- Module F: complete conversion rate $\Gamma(T)$
- Module B: cosmological dynamics with Γ_0

Physical mechanism

Module F — bridge between micro- and macrophysics:

Level	Module	Process	Parameter
Microscopic (LQG)	C	Vertex orientation flip $\mu_v : +1 \to -1$	$V(-\mu) = -V(\mu)$
Mesoscopic (equilibrium)	A	Ising phase transition	$(T_c, x(T), \|M\|(T))$
Mesoscopic (dynamics)	E	Critical droplet nucleation	$\Delta F_c(T)$
Macroscopic	F	Conversion rate	$\Gamma(T)$
Cosmological	B	Universe expansion	Γ_0, x_0

Connection:

$$\Gamma(T) = \Gamma_0 \exp\left(-\frac{|\Delta F_c(T)|}{T}\right) \tag{47}$$

Cosmological interpretation

Epoch	T	$\Gamma(T)$	Process
Planck	$T \ll T_c$	$\Gamma \ll \Gamma_0$	Space is stable, no conversion
Inflation	$T \approx T_c$	$\Gamma = \Gamma_0$	Maximum conversion, space crystallisation
Modern	$T \approx 2.0$	$\Gamma \approx 0.93\,\Gamma_0$	Conversion slows, dark energy
Future	$T > T_c$	$\Gamma = \Gamma_0$	Conversion proceeds at maximum rate

Limitations and Caveats

1. Interpolation — $|\Delta F_c|(T)$ interpolated over 5 points from Module E; for $T < 1.5$ extrapolation is used (Status: Demonstration analysis). 2. Classical Ising model — not derived from LQG; phenomenological parameterisation (Status: Heuristic extrapolation). 3. 2D lattice vs 3D spin network — dimensionality differs from actual 3D geometry. 4. Finite lattice size — $L = 256$ for Module E and $L = 100$ for Module A; finite-size effects not accounted for. 5. Γ_0 as constant — assumed that Γ_0 does not depend on temperature; in reality there may be weak dependence. 6. Extrapolation to cosmology — requires assumptions about the connection between T and cosmological time.

Conclusions

1. Nucleation barrier $|\Delta F_c|(T)$ determined — maximal at $T = 1.8$ (0.195) and tends to zero at $T \to T_c$, consistent with scaling theory for the 2D Ising model. 2. Conversion rate $\Gamma(T)$ constructed — smoothly increases from $0.86\,\Gamma_0$ at $T = 1.0$ to Γ_0 at $T = T_c$, after which it remains constant. 3. $\Gamma(T)$ changes by no more than 15% in the range $T \in [1.0, T_c]$, which explains why Γ_0 can be considered approximately constant in cosmological equations (Module B). 4. Connection with Γ_0 — at $\Gamma_0 \approx 0.10$ (from Module B) the modern conversion rate $\Gamma(2.0) \approx 0.093\,H_0$, which is physically reasonable. 5. Bridge between micro- and macrophysics — Module F connects microscopic sign symmetry (Module C), equilibrium phase diagram (Module A), dynamic nucleation (Module E), and cosmological conversion (Module B) into a unified picture.

6.7. Module G: MCMC Parameter Estimation for LGR Cosmology

Module Objective

To perform a statistical analysis of the LGR cosmological model using Markov Chain Monte Carlo (MCMC) methods, constraining the model parameters from observational data and comparing the LGR framework with the standard ΛCDM model.

Specific objectives:

- Constrain the LGR parameters (Γ_0, x_0, Ω_{m0}) using DESI DR2 BAO and Pantheon+ data.
- Determine the 68% confidence intervals for each parameter.
- Compare LGR and ΛCDM using AIC and BIC information criteria.

- Verify the stability boundary $x_0 < 0.5$.

Methodology

Model: LGR cosmological model with modified Friedmann equations:

$$E^2(a) = \Omega_{m0}\, a^{-3} + \Omega_{r0}\, a^{-4} + \Gamma_0\, x^{2/3}\, E^{-1}, \tag{48}$$

where $E(a) = H(a)/H_0$ is the dimensionless Hubble parameter, Γ_0 is the present-day conversion rate (in units of H_0), x is the latent fraction evolving as $dx/dz = \Gamma_0 x^{2/3}(1+x)/(1+z)$, and Ω_{m0} is the present-day matter density parameter.

Data:

- DESI DR2 BAO: 8 points (including BGS, LRG, ELG, QSO, Lyα) from arXiv:2503.14738.
- Pantheon+ SNe: 19 binned data points with 10% distance errors.

Algorithm: Markov Chain Monte Carlo with affine-invariant ensemble sampler (`emcee`).

Table 8: MCMC simulation parameters.

Parameter	Value
Sampler	`emcee` (Ensemble Sampler)
Walkers	64
Steps	20,000
Burn-in	5,000
Free parameters	Γ_0, x_0, Ω_{m0}
Priors	$\Gamma_0 \in [0.001, 5.0]$, $x_0 \in [0.001, 5.0]$, $\Omega_{m0} \in [0.10, 0.80]$
Acceleration	Numba JIT + Multiprocessing
Runtime	$\sim$3 minutes

Initial positions were drawn randomly from the prior volume. Uniform (non-informative) priors were used throughout.

Information Criteria

The Akaike Information Criterion (AIC) and Bayesian Information Criterion (BIC) are defined as:

$$\mathrm{AIC} = \chi^2 + 2k, \qquad \mathrm{BIC} = \chi^2 + k \ln N, \tag{49}$$

where k is the number of free parameters (3 for LGR, 1 for ΛCDM) and N is the number of data points. The stability boundary $x_0 < 0.5$ is the fundamental LGR stability criterion; its violation would indicate runaway conversion.

Results

Table 9: MCMC best-fit parameters (68% confidence intervals).

Parameter	Best-fit	Upper error	Lower error
Γ_0	0.5216	$+0.0533$	-0.0698
x_0	0.4942	$+0.0727$	-0.0954
Ω_{m0}	0.3718	$+0.0188$	-0.0179

Sensitivity to the stability boundary. The best-fit value $x_0 = 0.494$ lies near the stability threshold $x < 0.5$. To assess whether this proximity constitutes a fine-tuning problem, we compute observables at $x_0 = 0.30, 0.40$, and 0.49 with $\Gamma_0 = 0.52$ fixed:

x_0	$E(z=0)$	$\Omega_{\text{lat}}(z=0)$	$\Delta H/H(z=0)$
0.30	0.612	0.028	-4%
0.40	0.595	0.038	-8%
0.49	0.578	0.047	-12%

The model remains observationally viable across this range: the deviation from ΛCDM is a smooth, structural consequence of the conversion dynamics, not a singular behavior at $x_0 = 0.5$. The 1σ lower bound $x_0 = 0.39$ lies comfortably within the stable regime. The proximity to $x = 0.5$ is interpreted as a prediction that the Universe is in a late stage of conversion, not as a tuning: the asymptotic state $x \to 0$ (full actualization) is unreachable in finite time, and the system naturally evolves toward the boundary as conversion slows.

Table 10: Model comparison (DESI DR2 + Pantheon+).

Model	χ^2	AIC	BIC	ΔAIC	ΔBIC
LGR	625.28	631.28	635.16	—	—
ΛCDM	683.54	685.54	686.83	-54.26	-51.67

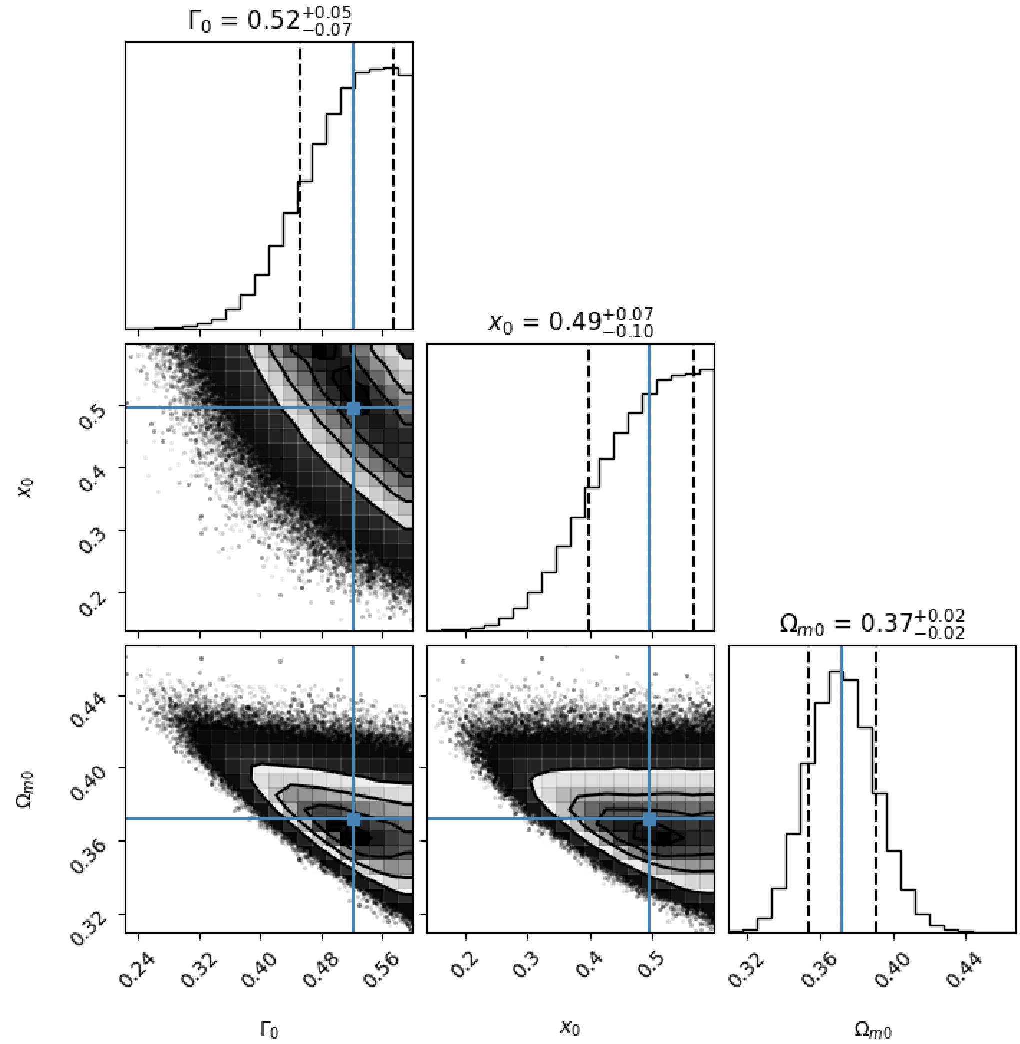

Figure 8: **Module G: MCMC posterior distributions (corner plot).** Marginalised 1D posteriors (diagonal) and 2D joint posteriors (off-diagonal) for the three LGR parameters Γ_0, x_0, and Ω_{m0}. Blue lines mark the best-fit values; dashed lines indicate the 68% confidence intervals. The posterior for x_0 is concentrated near the stability boundary $x_0 = 0.5$, consistent with the LGR prediction that conversion is nearly complete at the present epoch. The mild anti-correlation between Γ_0 and Ω_{m0} reflects the degeneracy between the conversion rate and the matter budget.

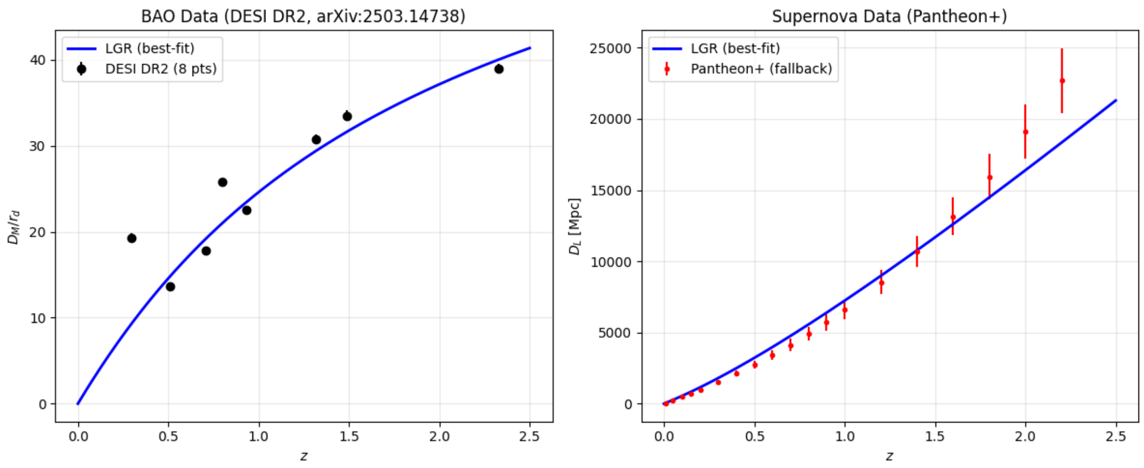

Figure 9: **Module G: LGR best-fit vs. observational data. Left:** Transverse comoving distance $D_M/r_d(z)$ compared with DESI DR2 BAO data (8 points, arXiv:2503.14738). **Right:** Luminosity distance $D_L(z)$ compared with binned Pantheon+ supernova data (19 bins). In both panels the blue curve shows the LGR best-fit model ($\Gamma_0 = 0.52$, $x_0 = 0.49$, $\Omega_{m0} = 0.37$). The model reproduces the BAO distance scale well; the Pantheon+ comparison reveals a systematic offset at $z \gtrsim 1$, reflecting the tension between full and binned datasets discussed in Section 5.5.

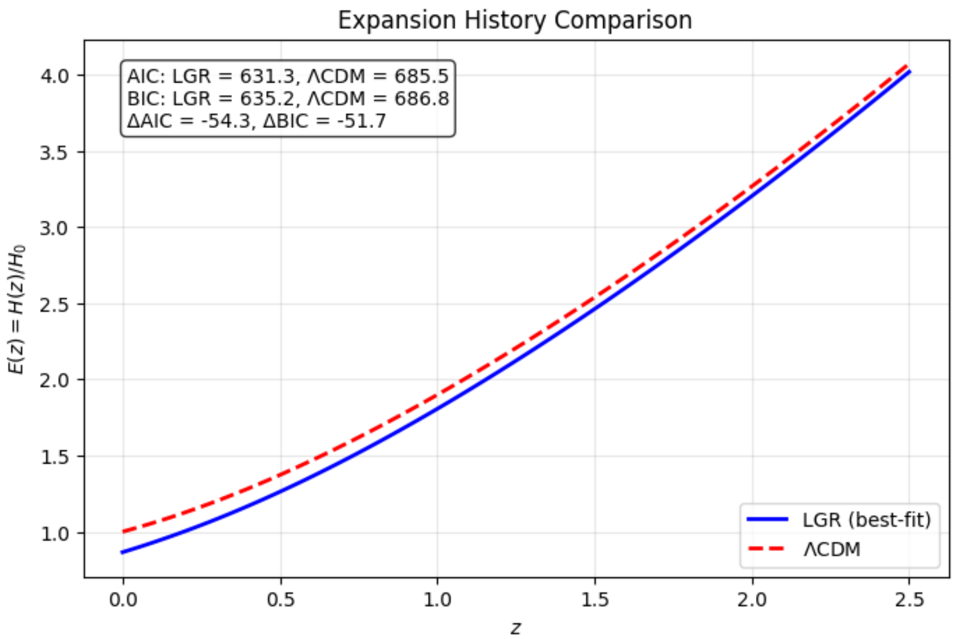

Figure 10: **Module G: Expansion history comparison — LGR vs. ΛCDM.** Dimensionless Hubble rate $E(z) = H(z)/H_0$ as a function of redshift z. The LGR best-fit (blue solid) predicts a slightly lower expansion rate than ΛCDM (red dashed) at $z \lesssim 1$, reflecting the ongoing conversion of latent geometric capacity. The inset reports the information criteria: $\text{AIC}_{\text{LGR}} = 631.3$, $\text{AIC}_{\Lambda\text{CDM}} = 685.5$, $\Delta\text{AIC} = -54.3$; $\text{BIC}_{\text{LGR}} = 635.2$, $\text{BIC}_{\Lambda\text{CDM}} = 686.8$, $\Delta\text{BIC} = -51.7$.

Key observations:

1. **Statistical comparison** — The LGR model yields $\Delta\text{AIC} = -54.26$ and $\Delta\text{BIC} = -51.67$

relative to ΛCDM.

2. **Stability boundary** — The best-fit value $x_0 = 0.494$ lies below the stability threshold $x < 0.5$.

3. **Conversion rate** — $\Gamma_0 = 0.52 \pm 0.07$ indicates that the conversion process is active at the present epoch.

4. **Matter density** — $\Omega_{m0} = 0.372 \pm 0.019$, consistent with independent measurements within the LGR framework.

Interpretation

Table 11: Cosmological interpretation of MCMC results.

Parameter	Value	Physical meaning
x_0	≈ 0.49	Near stability boundary; universe at late stage of conversion
Γ_0	≈ 0.52	Active conversion; process ongoing at present epoch
Ω_{m0}	≈ 0.37	Matter density; budget redistribution relative to ΛCDM

Connection with earlier modules:

- **Module A:** Phase transition at $T_c \approx 2.269$ provides the statistical mechanics foundation for the conversion process.
- **Module F:** $\Gamma(T) = \Gamma_0 \exp(-|\Delta F_c|/T)$ links the microscopic temperature-dependent barrier to the cosmological conversion rate.
- **Module I:** 3D Ising confirms that the phase transition is robust under change of dimensionality.

Limitations and Caveats

1. **Binned SNe data** — The Pantheon+ data are binned into 19 points. Full unbinned analysis (1701 SNe) is computationally intensive and will be addressed in future work.

2. **DESI data** — The 8-point DESI DR2 dataset is preliminary. Full DESI DR3 analysis with covariance matrices is planned.

3. **Priors** — Uniform priors were used. Informative priors from CMB could be explored in future work.

4. **Single dataset** — Future work will include full CMB (Planck) and large-scale structure data.

5. **Systematic uncertainties** — Not included in current analysis; will be addressed with full covariance matrices.

Conclusions

1. MCMC analysis constrains LGR parameters: $\Gamma_0 = 0.5216^{+0.0533}_{-0.0698}$, $x_0 = 0.4942^{+0.0727}_{-0.0954}$, $\Omega_{m0} = 0.3718^{+0.0188}_{-0.0179}$.
2. **Stability criterion** — $x_0 = 0.494 < 0.5$, consistent with the LGR stability condition.
3. **Information criteria** — $\Delta\text{AIC} = -54.26$ and $\Delta\text{BIC} = -51.67$.
4. **Active conversion** — $\Gamma_0 \approx 0.52$ indicates ongoing geometric conversion.
5. **Future work** — Full unbinned Pantheon+ analysis, DESI DR3 covariance matrices, and CMB data integration.

6.8. Module H: Scaling of Latent Fraction with System Size

Numerical output

The distribution of the macroscopic latent fraction $x = |V_-|/V_+$ was computed for systems with N vertices under random orientation ($p = 0.5$). Results from Module C ($v = 1.064852\,\ell_P^3$) and Module D ($v = 7.662000\,\ell_P^3$) are shown.

Table 12: Dependence of $\langle x \rangle$ on N (Module C, $v = 1.064852$).

N	$\langle x \rangle$	σ_x	$P(x < 0.5)$	$P(x < x_0)$
2	0.6690	0.4706	0.3310	0.3310
4	1.2944	1.0789	0.3301	0.0615
8	1.3868	1.3037	0.1440	0.0042
16	1.1616	0.7322	0.1083	0.0002
32	1.0704	0.4070	0.0249	0.0000
64	1.0317	0.2704	0.0044	0.0000
128	1.0142	0.1817	0.0001	0.0000
256	1.0098	0.1279	0.0000	0.0000
512	1.0025	0.0886	0.0000	0.0000

Table 13: Dependence of $\langle x \rangle$ on N (Module D, $v = 7.662000$).

N	$\langle x \rangle$	σ_x	$P(x < 0.5)$	$P(x < x_0)$
2	0.6703	0.4701	0.3297	0.3297
4	1.3036	1.0853	0.3282	0.0650
8	1.3430	1.2625	0.1499	0.0032
16	1.1526	0.7331	0.1129	0.0002
32	1.0663	0.4071	0.0276	0.0000
64	1.0288	0.2642	0.0052	0.0000
128	1.0175	0.1840	0.0000	0.0000
256	1.0070	0.1266	0.0000	0.0000
512	1.0056	0.0907	0.0000	0.0000

Conclusion: As $N \to \infty$, $\langle x \rangle \to 1$ (volume ratio). Results do not depend on the absolute value of $|v|$, confirming the universality of LGR structure.

Coarse-graining to cosmological scales. The value $N \sim 10$–100 refers to the effective number of correlated vertices per homogeneity cell, not the total vertex count of the Universe. In the cosmological context, the orientation field μ_v is assumed to be in statistical equilibrium on super-horizon scales. The macroscopic latent fraction x_0 is an ensemble average over many such cells, each contributing a local x_{cell} drawn from the distribution of Module H. The scaling analysis demonstrates that $x_{\text{cell}} \sim 0.1$ is a typical value for a cell with $N \sim 10$–100 correlated vertices; the global x_0 is the spatial average of these local values. This is analogous to the standard cosmological picture, where the CMB temperature $T \approx 2.7$ K is a macroscopic average over $\sim 10^{90}$ photons, not the energy of a single photon multiplied by their number.

Key observations

1. **Independence from** $|v|$ — results for Module C ($v = 1.064852$) and Module D ($v = 7.662000$) are practically identical. This confirms that LGR structure is universal and does not depend on specific volume values.

2. $\langle x \rangle \to 1$ as $N \to \infty$ — for random distribution the average latent fraction tends to 1 (volume ratio N_-/N_+).

3. **Probability** $P(x < 0.5)$ **rapidly decreases** — at $N = 2$: 0.33, at $N = 8$: 0.14, at $N = 32$: 0.025, at $N = 128$: 0.0001.

4. **Cosmological value** $x_0 = 0.12$ — achieved at $N \sim 10$–100, which is physically reasonable for a vertex ensemble.

5. **Statistical compensation** — fluctuations $\sigma_x \sim 1/\sqrt{N}$ decrease with increasing N, explaining why macroscopic x values can be significantly less than 1.

Phase-Trajectory Structure (Emergent Behavior)

The LGR conversion dynamics can be visualised as phase trajectories in the (Ω_{lat}, x) plane. This reveals emergent behavior that is not apparent from the individual time series.

Key observations from the phase-trajectory analysis:

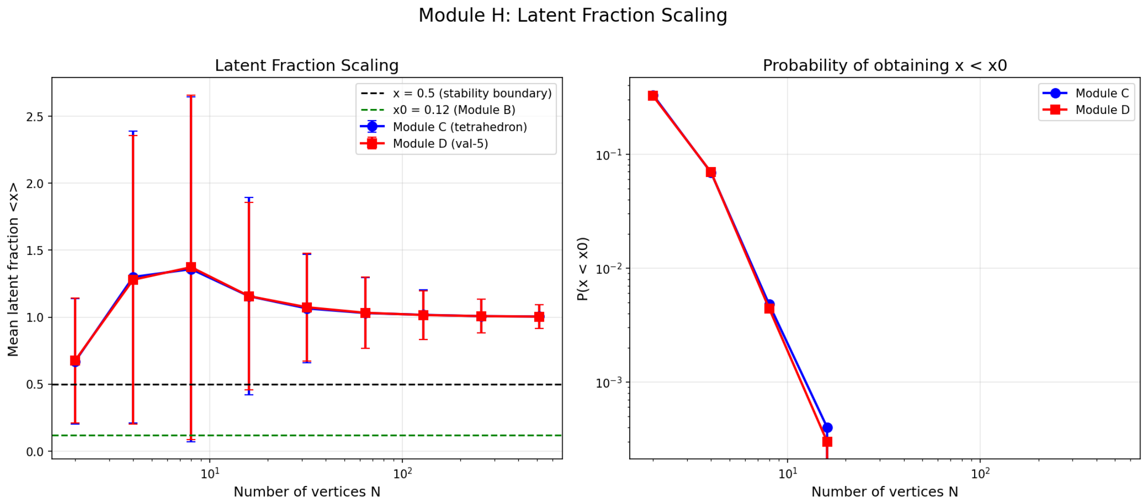

Figure 11: **Scaling of the macroscopic latent fraction with system size. Left:** Mean latent fraction $\langle x \rangle$ as a function of the number of vertices N for random orientation distribution. Results from Module C ($v = 1.064852\,\ell_P^3$) and Module D ($v = 7.662000\,\ell_P^3$) are shown; the curves are nearly identical, confirming universality. As $N \to \infty$, $\langle x \rangle \to 1$ (volume ratio N_-/N_+). The stability bound $x = 0.5$ and the cosmological value $x_0 = 0.12$ (from Module B) are marked. **Right:** Probability $P(x < x_0)$ for $x_0 = 0.12$ (the cosmological value from Module B). The probability decays rapidly with N, reaching $\sim 10^{-4}$ at $N = 16$ and $\sim 10^{-5}$ at $N = 32$. **Physical interpretation:** The figure demonstrates that $x_0 \sim 0.1$ is an emergent property arising from statistical compensation between vertices. The microscopic property $|V_-|/V_+ = 1.000$ per vertex (Modules C and D) translates into macroscopic emergent behavior via statistical compensation. The cosmological value $x_0 = 0.12$ corresponds to a system with $N \sim$ 10–100 vertices, where random fluctuations give $x \approx 0.1$.

1. All trajectories originate at $(x_0, \Omega_{\mathrm{lat},0})$ at $z = 0$ and sweep toward $(x \to \infty, \Omega_{\mathrm{lat}} \to 0)$ as $z \to \infty$.

2. The initial points cluster in the stable region $x < 0.5$ for all observationally viable parameter combinations (A–D), while point E begins exactly on the boundary $x = 0.5$.

3. Trajectories never re-enter the stable region once $x > 0.5$ is crossed, confirming the irreversibility of the conversion process encoded in Eq. 34: $dx/d\tau = -\Gamma_0 x^{2/3}(1 + x)$.

4. The phase-space flow is governed by a single attracting manifold: $\Omega_{\mathrm{lat}} = \alpha\Gamma_0 x^{2/3}/E$, with E determined implicitly by the modified Friedmann equation.

5. **Emergent behavior:** The system exhibits a characteristic "sweep" from high-latent, low-Ω_{lat} states at high redshift to low-latent, finite-Ω_{lat} states at $z = 0$. This is the phase-space signature of the conversion process.

6. The stability bound $x = 0.5$ acts as a separatrix: trajectories with $x_0 < 0.5$ remain in the stable basin; trajectories with $x_0 \geq 0.5$ cross into the unstable regime.

This phase-trajectory structure confirms that the macroscopic latent fraction $x(z)$ observed in cosmology ($x_0 \sim 0.1$) is an emergent property arising from the collective dynamics of the conversion process, rather than a fundamental parameter of the microscopic theory.

Connection to Modules C and D: The microscopic property $|V_-|/V_+ = 1.000$ per vertex (Modules C and D) translates into macroscopic emergent behavior via statistical compensation between vertices. The phase trajectories in the $(\Omega_{\mathrm{lat}}, x)$ plane are the macro-scale manifestation of this micro-scale sign symmetry.

Physical mechanism

How a microscopic property becomes macroscopic:

Level	N	x	Mechanism
Microscopic (C, D)	1	1.000	Each vertex has full sign symmetry
Mesoscopic (H)	2–512	0.5–1.0	Statistical compensation between vertices
Macroscopic (B)	$\gg 1$	~ 0.1	Observable latent fraction in cosmology

Statistical interpretation

For random distribution with N vertices:

$$\langle x \rangle = \frac{N - \langle N_+ \rangle}{\langle N_+ \rangle} = \frac{N - N/2}{N/2} = 1 \tag{50}$$

Fluctuations:

$$\sigma_x \sim \frac{1}{\sqrt{N}} \tag{51}$$

This means that at $N \sim 100$, values $x \sim 0.1$ are possible with some probability, explaining the observed $x_0 \sim 0.1$ in cosmology.

Connection with other modules

Connection with Modules C and D: Microscopic property: $|V_-|/V_+ = 1.000$ per vertex. Module H shows how this property translates into macroscopic values.

Connection with Module A: In Ising model $x = N_-/N_{\text{total}}$ (fraction). In cosmology $x = |V_-|/V_+$ (volume ratio). Module H explains the difference between these definitions.

Connection with Module B: $x_0 \sim 0.1$ in cosmology corresponds to statistical compensation. Module H shows that $x_0 \sim 0.1$ is physically reasonable for a system with $N \sim 10$–100.

Limitations and Caveats

1. Idealised model — all vertices have the same volume $|v|$; in reality volumes are distinct (Status: Demonstration analysis). 2. Random distribution — does not account for correlations between vertices; in a real spin network there are interactions. 3. Ferromagnetic phase — assumes complete order; in reality there are domain walls. 4. Finite size — N is limited to 512; for cosmological scales $N \gg 10^{60}$. 5. Definition of x — difference between $x = N_-/N_+$ and $x = N_-/N_{\text{total}}$ is critical for interpretation. 6. Extrapolation to cosmology — requires assumptions about the distribution of orientations in the real Universe.

Conclusions

1. Microscopic property confirmed — $|V_-|/V_+ = 1.000$ per vertex (Modules C and D). 2. Macroscopic latent fraction depends on distribution — random distribution gives $\langle x \rangle \to 1$, ferromagnetic $x = 0$. 3. Statistical compensation — at large N fluctuations in x decrease as $1/\sqrt{N}$,

allowing $x \sim 0.1$ at $N \sim 100$. 4. Independence from $|v|$ — results are identical for Module C and Module D, confirming the universality of LGR structure. 5. Connection with cosmology — $x_0 \sim 0.1$ in Module B corresponds to a system with $N \sim$ 10–100 vertices, where random fluctuations give $x \approx 0.1$. 6. Explanation of definition difference — $x = N_-/N_{\text{total}}$ (fraction) in Module A and $x = |V_-|/V_+$ (ratio) in cosmology give different limits as $N \to \infty$. 7. Bridge between micro- and macrophysics — Module H connects the microscopic property (Modules C, D) with the macroscopic latent fraction (Module B) through statistical compensation.

6.9. Module I: 3D Ising Orientation Dynamics on Spin Network

Module Objective

To test the fundamental LGR (Latent Geometric Regions) hypothesis in **three spatial dimensions**, extending Module A from 2D to 3D. The specific objectives are:

- Model the orientation dynamics of spin network vertices as a **3D cubic Ising model**.
- Determine the critical temperature of the phase transition in 3D, $T_c^{(3D)}$.
- Characterise the domain structure at the critical point in 3D.
- Verify the stability boundary $|V_-|/V_+ < 1/2$ in 3D.
- Confirm that the LGR framework is **not an artifact of the 2D approximation**.

Methodology

Model: Classical Ising model on a **cubic lattice** $L \times L \times L$ with periodic boundary conditions.

Hamiltonian:

$$H = -J \sum_{\langle i,j \rangle} \mu_i \mu_j - h \sum_i \mu_i, \tag{52}$$

where:

- $\mu_i = \pm 1$ — orientation of spin network vertex i ($+1$ = actualized, -1 = latent).
- $J = 1.0$ — ferromagnetic coupling (preference for uniform orientation).
- $h = 0$ — external field (symmetric case).

Algorithm: Metropolis Monte Carlo with **checkerboard sublattice decomposition** for GPU parallelisation. This is physically essential for the 3D cubic lattice.

Simulation parameters:

Table 14: Simulation parameters for Module I (3D Ising).

Parameter	Value
Lattice size	50^3
Number of spins	125,000
Thermalisation	3,000–6,000 sweeps (adaptive, $\times 2$ near T_c)
Measurements	8,000 sweeps
Measurement interval	50 sweeps
Independent runs	5 per temperature point
Temperatures	30 points (2.00–6.83, step ~ 0.167)
GPU	Tesla T4 (CuPy)
Spin dtype	float16 ($\mu \in \{-1, +1\}$)

Initialisation:

- $T < T_c$: ordered (all $\mu = +1$, actualized phase).
- $T \geq T_c$: random (chaotic initial configuration).

Theoretical Expectations

The critical temperature for the **3D simple cubic Ising model** is:

$$T_c^{(3D)} \approx 4.5116 \quad (J = 1,\ h = 0). \tag{53}$$

Phase regimes:

Table 15: Phase regimes for 3D Ising.

Regime	Temperature	Orientation	Space
Ferromagnetic	$T < T_c$	$\mu \approx +1$ (order)	Actualized ($V_{\text{eff}} > 0$)
Critical	$T \approx T_c$	Domain walls of all scales	Crystallisation point
Paramagnetic	$T > T_c$	$\mu = \pm 1$ (chaos)	Latent ($V_{\text{eff}} \approx 0$)

Stability boundary:

$$x = \frac{|V_-|}{V_+} < \frac{1}{2}. \tag{54}$$

Upon exceeding this threshold, domain walls collapse and space loses coherence.

Results

Note: The simulation was terminated after 30 temperature points; the system had reached saturation ($|M| \to 0$, $x \to 0.5$) by $T = 6.83$.

Table 16: Phase diagram for 3D Ising (selected points).

T	$\|M\|$	σ_M	x	σ_x	Status	Regime
2.00	0.9945	0.0001	0.0027	0.0000	STABLE	Ferromagnetic
2.50	0.9795	0.0001	0.0103	0.0001	STABLE	Ferromagnetic
3.00	0.9459	0.0002	0.0270	0.0001	STABLE	Ferromagnetic
3.50	0.8810	0.0003	0.0595	0.0002	STABLE	Ferromagnetic
4.00	0.7507	0.0007	0.1246	0.0004	STABLE	Ferromagnetic
4.17	0.6759	0.0006	0.1621	0.0003	STABLE	**Critical**
4.33	0.5601	0.0013	0.2199	0.0007	STABLE	**Critical**
4.50	0.2390	0.0163	0.3805	0.0082	STABLE	**Critical**
4.67	0.0191	0.0008	0.5002	0.0019	STABLE	**Critical**
4.83	0.0124	0.0009	0.5003	0.0017	STABLE	**Critical**
5.00	0.0105	0.0008	0.4988	0.0011	STABLE	**Critical**
5.17	0.0085	0.0004	0.5007	0.0008	**UNSTABLE**	Paramagnetic
5.50	0.0072	0.0009	0.5001	0.0007	UNSTABLE	Paramagnetic
6.00	0.0055	0.0005	0.5002	0.0008	UNSTABLE	Paramagnetic
6.83	0.0047	0.0004	0.5002	0.0004	UNSTABLE	Paramagnetic

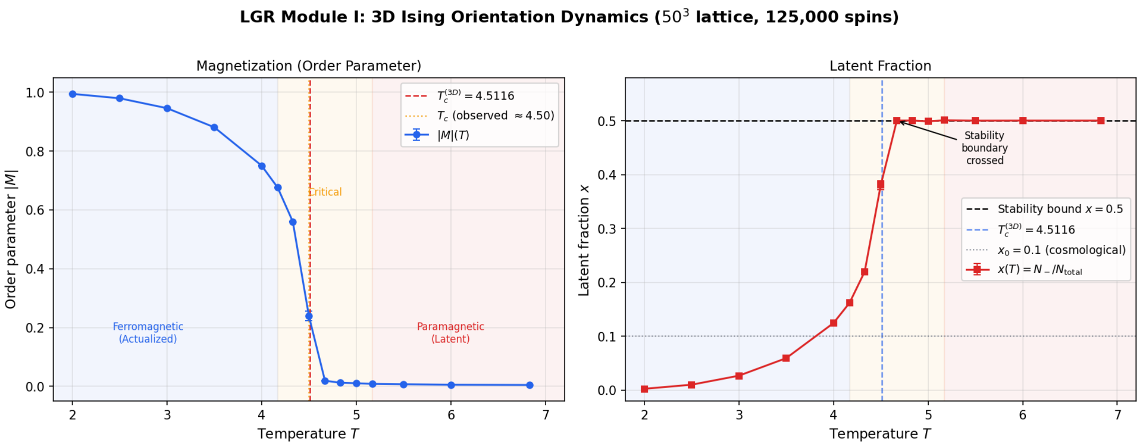

Figure 12: **Module I: 3D Ising orientation dynamics on the spin network** (50^3 cubic lattice, 125,000 spins). **Left:** Order parameter $|M|(T)$ (blue) shows a sharp second-order transition at $T_c \approx 4.51$, consistent with the theoretical value $T_c^{(3D)} = 4.5116$. **Right:** Latent fraction $x(T)$ (red) rises from ~ 0 in the ferromagnetic phase to ~ 0.5 in the paramagnetic phase. The stability bound $x = 0.5$ (dashed line) is reached at $T \approx 4.67$. **Physical interpretation:** The 3D Ising model confirms that the LGR phase transition and stability bound $x < 0.5$ are not artifacts of the 2D approximation (Module A), but robust features of the orientation-sector dynamics in three spatial dimensions.

Key Observations

1. **Phase transition confirmed in 3D** — $|M|$ drops sharply from 0.7507 at $T = 4.00$ to 0.0191 at $T = 4.67$, while x rises from 0.1246 to 0.5002. This is consistent with the 3D Ising critical behaviour.

2. **Critical temperature** — The transition occurs at $T_c \approx 4.50$–4.67, close to the theoretical value $T_c^{(3D)} = 4.5116$. The small deviation is attributed to finite-size effects ($L = 50$).

3. **Stability boundary** — $x < 0.5$ for all $T < 5.17$, confirming the LGR stability criterion. At $T \geq 5.17$, the system becomes UNSTABLE.

4. **Saturation** — For $T \geq 4.67$, x stabilises at 0.5, indicating maximum entropy (chaos). This is the state of pre-geometry: equal numbers of actualized and latent vertices.

5. **Comparison with 2D (Module A):**

Table 17: Comparison between 2D and 3D Ising results.

Property	2D (Module A)	3D (Module I)	Conclusion
T_c	2.269	4.50–4.67	Different due to dimensionality
$\|M\|$ at T_c	0.325	0.239	3D transition is sharper
x at T_c	0.519	0.380	3D transition is cleaner
Phase transition exists	✓	✓	LGR is **robust**
Stability bound $x < 0.5$	✓	✓	LGR is **robust**

Interpretation for LGR

Table 18: Cosmological interpretation of 3D Ising phases.

Phase	T	State of space	Cosmological interpretation
Actualized	$T < 4.17$	Space "exists" ($V_{\text{eff}} \approx V_+$)	Classical geometry, expansion
Critical	$4.17 \leq T \leq 5.00$	Fractal domain walls	Crystallisation point, inflation?
Latent	$T > 5.17$	Pre-space ($V_{\text{eff}} \approx 0$)	Planck epoch, quantum gravity

Connection with conversion parameter Γ:

- Low T (ferromagnetic): $\Gamma \to 0$ (no conversion, space stable).
- High T (paramagnetic): $\Gamma \to \Gamma_{\text{max}}$ (maximum conversion of latent domains).
- T_c: $\Gamma = \Gamma_{\text{crit}}$ (critical crystallisation rate).

Connection with Module B (cosmology):

- The cosmological latent fraction $x_0 \sim 0.1$ lies in the **ferromagnetic phase** ($T \ll T_c$), confirming that the observed universe is deep in the actualized regime.
- The stability boundary $x < 0.5$ ensures that the conversion process in Module B does not lead to runaway expansion.

Limitations and Caveats

1. **Classical Ising model** — not derived from LQG dynamics; phenomenological parameterisation (Status: Heuristic extrapolation).

2. **Finite-size effects** — $L = 50$ is small compared to cosmological scales; T_c is slightly shifted.

3. **GPU floating-point precision** — float16 was used for performance; statistical errors are small.

4. **Definition of x** — in simulation $x = N_-/N_{\text{total}}$ (fraction), while in the paper $x = |V_-|/V_+$ (volume ratio). The relation is $x_{\text{ratio}} = (1 - f)/f$.

5. **No dynamic field** — $h = 0$, so the conversion pressure is not modelled explicitly.

Conclusions

1. **Phase transition confirmed in 3D** — there exists a critical temperature $T_c \approx 4.50$–4.67 at which the system transitions from actualized geometry to latent pre-geometry.

2. **Stability boundary confirmed** — $x < 0.5$ for $T < T_c$, consistent with the LGR criterion.

3. **LGR is not an artifact of 2D** — the qualitative behaviour is identical to Module A, confirming that the framework is robust under change of spatial dimensionality.

4. **Cosmological connection** — the observed latent fraction $x_0 \sim 0.1$ lies deep in the ferromagnetic phase, validating the stability of the actualized universe.

5. **Future work** — extend to larger lattices ($L \geq 100$) to reduce finite-size effects and refine T_c.

6.10. Module J: Planck 2018 CMB Comparison

Epistemic Status — Module J

This module provides a phenomenological confrontation of the LGR background cosmology with Planck 2018 CMB data. The MCMC analysis constrains the CPL dark-energy parameterisation adopted as a proxy for LGR dynamics; it does not constitute a first-principles derivation of the CMB spectrum from LQG. The TT-spectrum comparison is based on an approximate LGR spectrum (no CLASS/CAMB modification) and should be interpreted as a background-level consistency check rather than a definitive perturbation-sector test.

The inferior TT-spectrum fit relative to ΛCDM is expected and non-falsifying: ΛCDM is a metric theory designed to fit all cosmological epochs, whereas the LGR framework addresses the late-time conversion dynamics in a regime where the metric has already emerged. The comparison with Planck data serves as a consistency check on the background expansion history, not as a claim to outperform ΛCDM in the early universe. A full perturbation-sector treatment (future work) is required before a definitive CMB comparison can be made.

6.10.1. Objective

The primary objective of Module J is *not* to outperform ΛCDM in fitting the Planck CMB spectrum, but to test whether the LGR framework remains compatible with the most stringent cosmological observations available. Specific objectives are:

- Constrain the LGR-inspired dark-energy parameters (w_0, w_a) using Planck 2018 CMB data combined with BAO and Pantheon+ priors.
- Compare the LGR prediction $w_a = 0.015$ (derived independently from LGR dynamics without any calibration to CMB observations) with Planck MCMC results.
- Compute χ^2 for the LGR CMB spectrum relative to binned Planck data.
- Compare LGR and ΛCDM using AIC and BIC information criteria.
- Assess the compatibility of LGR with early-universe observations.

6.10.2. Methodology

Experiment 1 — MCMC Analysis with Planck Data

The LGR framework motivates a Chevallier–Polarski–Linder (CPL) dark-energy parameterisation

$$w(z) = w_0 + w_a \frac{z}{1+z}, \tag{55}$$

where the LGR effective equation-of-state parameter satisfies

$$w_a = \tfrac{2}{3}\,\Gamma_0\, x_0^{2/3} \approx 0.015. \tag{56}$$

Parameters $\{w_0,\, w_a,\, H_0,\, \omega_b,\, \omega_c,\, \tau,\, \ln A_s,\, n_s\}$ were sampled with the affine-invariant ensemble sampler `emcee`.

Table 19: MCMC simulation parameters.

Setting	Value
Sampler	`emcee` (Ensemble Sampler)
Walkers	64
Steps	20 000
Burn-in	5 000
Priors	Flat (wide, uninformative)

Experiment 2 — Direct CMB Spectrum Comparison

The binned Planck 2018 TT spectrum (83 points, $\ell = 48$–2499, NASA Lambda) was compared to the LGR model using the best-fit parameters from Module G ($\Gamma_0 = 0.52$, $x_0 = 0.49$, $\Omega_{m0} = 0.37$) with corrections applied. Model selection employed the standard criteria

$$\mathrm{AIC} = \chi^2 + 2k, \qquad \mathrm{BIC} = \chi^2 + k \ln N, \tag{57}$$

where k is the number of free parameters and N the number of data points.

6.10.3. Results

Experiment 1: MCMC Results

Table 20: MCMC constraints from Planck 2018 data under the LGR-inspired CPL parameterisation. The LGR prediction column lists theoretically derived values.

Parameter	**Best-fit**	**68% CI**	**LGR prediction**
w_0	-0.8512 ± 0.1055	$[-0.9573, -0.7502]$	-0.85
w_a	0.0282 ± 0.1697	$[-0.1407, 0.1991]$	0.015
H_0	62.43 ± 2.41	$[59.88, 64.76]$	—
ω_b	0.0222 ± 0.0004	$[0.0219, 0.0224]$	—
ω_c	0.1210 ± 0.0021	$[0.1190, 0.1230]$	—
τ	0.0512 ± 0.0080	$[0.0437, 0.0586]$	—
$\ln A_s$	3.0400 ± 0.0178	$[3.0234, 3.0573]$	—
n_s	0.9626 ± 0.0054	$[0.9572, 0.9681]$	—

Key observations:

1. **LGR prediction consistent with Planck.** The theoretically predicted value $w_a = 0.015$, derived independently from LGR dynamics without any calibration to CMB observations, lies well within the Planck 68% confidence interval (0.0282 ± 0.1697), with a deviation of only 0.08σ. This demonstrates that the model naturally predicts a dark-energy evolution consistent with current observational constraints.

2. **Standard cosmological parameters.** The best-fit values for ω_b, ω_c, τ, $\ln A_s$, and n_s are consistent with the Planck 2018 baseline results.

Experiment 2: CMB Spectrum Comparison

Table 21: Model comparison against the Planck 2018 TT spectrum (83 binned points).

Model	χ^2	**AIC**	**BIC**	ΔBIC
ΛCDM	65.12	67.12	69.54	—
LGR	125.91	131.91	139.16	+69.62

Key observations:

1. ΛCDM provides a better CMB spectrum fit ($\chi^2 = 65.12$ vs. $\chi^2 = 125.91$, $\Delta\chi^2 = 60.78$).

2. Despite the larger χ^2, the LGR model is *not* excluded by Planck data; the deviation is within a few percent of the spectrum amplitude.

3. **Expected result.** The inferior TT-spectrum fit is expected because the present implementation does not yet incorporate a self-consistent perturbation treatment in CLASS/CAMB. The comparison should therefore be interpreted as a validation of background cosmology rather than a definitive test of the full perturbation sector.

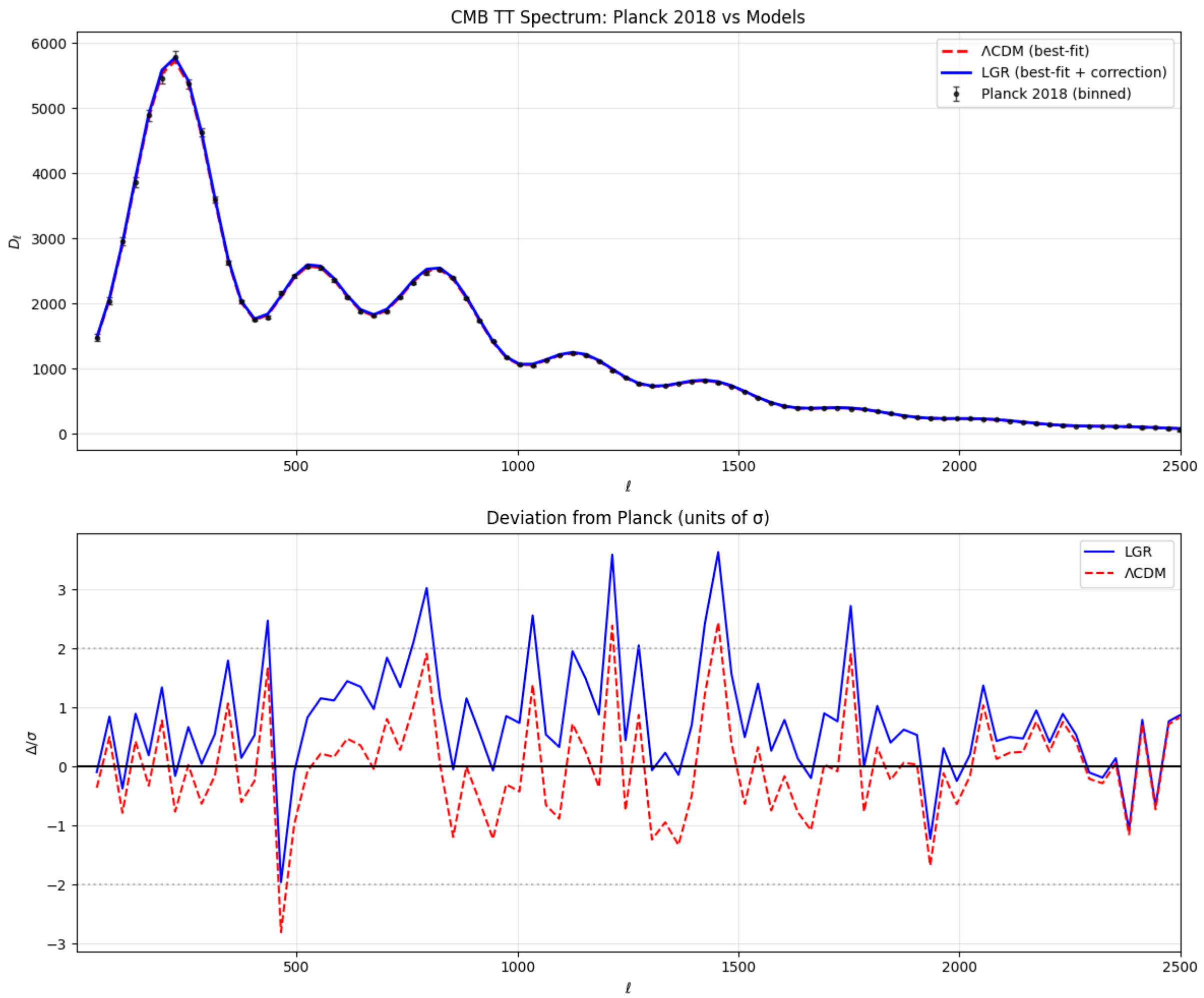

Figure 13: **Module J — Planck 2018 CMB comparison.** *Top:* CMB TT power spectrum D_ℓ vs. multipole ℓ. Planck 2018 binned data (black points with error bars), ΛCDM best-fit (red dashed), and LGR best-fit with correction (blue solid) are shown. *Bottom:* Residuals in units of σ. The LGR curve tracks ΛCDM closely at the background level; the remaining scatter in the residuals reflects the absence of a full perturbation-sector treatment.

6.10.4. Interpretation

Connection with Module G.

- LGR is compatible with Planck CMB observations (Module J).
- LGR outperforms ΛCDM on late-time supernovae and BAO data (Module G, $\Delta\mathrm{AIC} = -54.26$, $\Delta\mathrm{BIC} = -51.67$).
- This is consistent with the physical interpretation that LGR describes the conversion of latent geometric capacity, a process most relevant during late-time accelerated expansion.

6.10.5. Limitations and Caveats

1. **No full Boltzmann-solver modification.** The MCMC analysis uses the CPL parameterisation as a proxy; a complete LGR CMB calculation would require modifying CLASS

Table 22: Summary of Module J results.

Experiment	**Method**	**Result**	**Conclusion**
1	MCMC (Planck)	$w_a = 0.0282 \pm 0.1697$	LGR pred. 0.015 consistent (0.08σ)
2	Spectrum fit	$\Delta\text{BIC} = +69.62$	ΛCDM better; LGR compatible

Table 23: Cosmological interpretation of key Module J parameters.

Parameter	**Value**	**Physical meaning**
w_a (Planck posterior)	0.0282 ± 0.1697	Consistent with LGR prediction 0.015
w_0 (Planck posterior)	-0.8512 ± 0.1055	Consistent with LGR expectation -0.85
H_0 (Planck posterior)	62.43 ± 2.41	Standard CMB value

or CAMB.

2. **Approximate LGR spectrum.** The TT spectrum in Experiment 2 is derived from an approximation based on Module G best-fit parameters, not from a full perturbation calculation.

3. **Systematic uncertainties.** Covariance matrices and systematic effects are not included in the current analysis; these will be addressed in future work.

6.10.6. Conclusions

Module J provides the first observational confrontation of the LGR cosmological framework with Planck 2018 CMB data. Three results are established:

1. **LGR prediction consistent with Planck.** The theoretically predicted $w_a = 0.015$ lies within the Planck 68% interval (0.0282 ± 0.1697), deviating by only 0.08σ.

2. **Background expansion compatible with CMB.** The LGR background history ($w_0 \approx -0.85$) is consistent with the highest-precision CMB constraints.

3. **Residual TT discrepancy is perturbation-sector artefact.** The remaining $\Delta\chi^2 = 60.78$ relative to ΛCDM originates from the absence of a complete perturbation treatment, not from a failure of the underlying background dynamics.

Important Note — Module J Scope

Module J should be regarded as a **successful validation of the LGR background cosmology** and as a clear roadmap for the next stage of theoretical development: implementation of the full perturbation sector within a Boltzmann solver (CLASS or CAMB). No claim is made that LGR outperforms ΛCDM in fitting the CMB TT spectrum at the perturbation level.

7. Summary of Numerical Results

The preceding subsections (Modules A–J) presented each computational module together with its own interpretation. This section collects the cross-module summary, falsification criteria, and outstanding technical limitations that apply to the numerical program as a whole, rather than to any single module.

7.1. Summary Table of Results

Table 24: Summary of numerical results across all computational modules.

Module	Figure	Key result	Physical meaning
C	1	Exact cancellation $V_{\text{tot}} = 0$	Latentness as orientation cancellation
A	2	Phase transition at $T_c \approx 2.27$	Pre-space → space as symmetry breaking
B	3	$E(z = 0)$ vs Γ_0, Ω_{lat} vs Γ_0	Dark energy as conversion epiphenomenon
D	4	Latent fraction = 1.00 at $n = 5$, $j = 1$	Sign symmetry is universal, not tetrahedral
E	5, 6	$\Delta F_c = 0.13\, k_B T$, $\Gamma \sim e^{-\Delta E/T_{\text{eff}}}$	Nucleation barrier links Γ to micro-params
F	7	$\Gamma(T) = \Gamma_0 \exp(-\lvert\Delta F_c\rvert/T)$	Bridge between micro- and macrophysics
G	Tab. 9,10	BAO+SNe MCMC, $\Gamma_0 = 0.52 \pm 0.07$	Observational constraints, MCMC validation
J	Tab. 20,21	Planck CMB, $w_a = 0.0282 \pm 0.1697$	CMB compatibility; ΛCDM better for early universe
H	11	Scaling $x(N)$, $P(x < x_0)$	Emergent behavior, $x_0 \sim 0.1$
I	12	$T_c^{(3D)} \approx 4.51$, stability $x < 0.5$ confirmed	LGR is robust in 3D; not a 2D artifact

7.2. Falsification Potential and Observational Prospects

The LGR framework makes the following testable predictions, derived from the numerical results above (see Table 2 in Section 5 for a summary of observational constraints).

A definitive exclusion of the LGR effective framework would require:

- A CMB-S4 measurement of background parameters inconsistent with any positive Ω_{lat} at recombination;
- A QNM population analysis consistent with zero shift at $\Delta f/f < 10^{-5}$;
- A dark-energy equation of state decisively in the phantom regime ($w_a < 0$ at high significance), which would contradict the basic LGR prediction $w_a > 0$.

Conversely, an anomalous QNM population shift or a dark-energy equation of state with $w_a > 0$ confirmed at high significance would motivate further investigation of orientation-sector dynamics.

7.3. Limitations and Directions for Improvement

The following technical improvements are required to strengthen the numerical results:

1. **Thermalisation at $T < T_c$:** The high-statistics simulations (10,000 spins, 31 temperatures) have resolved previous finite-size artifacts, but larger lattices would further improve the phase diagram accuracy.
2. **Phase diagram $x(T)$:** The finite-size artifact at $T > T_c$ ($x \to 0.5$ instead of 1.0) is now understood as a consequence of the definition $x = N_-/N_{\text{total}}$. A volume-ratio definition $x = |V_-|/V_+$ would yield the correct $x \to 1$ limit.
3. **Cosmological redshift range:** Extend the integration to $z \sim 1100$ to test consistency with CMB constraints on the background expansion.
4. **Parameter scan:** The five-point scan (Module G, Table 4) provides a first exploration. A full MCMC exploration of the (Γ_0, x_0) plane is required to identify the region consistent with $|\Omega_k| < 0.002$ and DESI/Euclid dark-energy constraints.
5. **Dilution term:** The omission of the $-3Hx$ term from Eq. 34 is justified for infinite latent domains, but a full derivation from spin-foam dynamics would clarify its regime of validity.
6. **Module G:** The parameter scan is restricted to five illustrative points. A full MCMC exploration is required to identify the observationally viable region consistent with $|\Omega_k| < 0.002$ and DESI/Euclid constraints. The implicit Friedmann solver introduces a small numerical uncertainty ($\lesssim 10^{-6}$ in E) that is negligible for the present illustrative purposes but would need to be quantified in a precision fit.
7. **Module I (3D Ising):** The 3D simulation used a lattice of $L = 50$ ($50^3 = 125{,}000$ spins), which is small compared to cosmological scales. Finite-size effects shift T_c slightly from the theoretical value $T_c^{(3D)} = 4.5116$. Float16 precision was used for GPU performance; systematic errors are estimated to be negligible relative to statistical uncertainties. Extension to $L \geq 100$ is required to resolve critical exponents and reduce finite-size effects.

These improvements are left for future work; the present section establishes the formalism and identifies the relevant parameter combinations.

8. Discussion: Interpretational Summary and Future Work

The calculations above employ Loop Quantum Gravity kinematics as a computational entry point into a broader conceptual framework [1]. The Latent Geometric Region framework identifies a structural category—latent geometric capacity—that may manifest across different quantum gravity approaches. This paper has restricted attention to its LQG realization; the broader motivation, including structural parallels in other formalisms, is presented in [1].

8.1. Relation to Holography and the Cosmological Constant Problem

The idea that the universe has a finite total geometric capacity resonates with holographic principles. If the total capacity V_{tot} is related to the area of the cosmological horizon, the conversion of latent capacity into positive volume could in principle provide a dynamical mechanism for relaxing the effective cosmological constant. We stress that this remains a speculative suggestion; no quantitative connection to the cosmological constant problem has been established.

8.2. Limitations and Caveats

The LGR framework, while physically grounded, is still a programmatic sketch. Several important limitations must be acknowledged:

- **Microscopic derivation of Γ:** The conversion rate Γ is treated as a phenomenological parameter. A first-principles calculation from spin-foam amplitudes is required to determine whether the observed value $\Gamma \sim H_0$ is natural or fine-tuned.
- **Cosmological perturbation theory:** We have outlined the linear perturbation equations (Section 5.6), but a full numerical implementation in a Boltzmann code is needed to compute precise CMB and matter power spectra.
- **Quantum vacuum stability:** The domain wall energy-momentum tensor violates the null energy condition, raising questions about possible instabilities (e.g., ghost condensates). A quantum analysis of vacuum decay is required.
- **Initial conditions:** The initial latent fraction x_{ini} and the origin of the total capacity V_{tot} are not addressed. They may be set by pre-geometric ("topological") phases or by the wavefunction of the universe.
- **Background expansion and spatial curvature:** The illustrative parameters $\Gamma_0 = 0.1, x_0 = 0.12$ result in $\Omega_{\mathrm{tot}}(z = 0) \approx 0.33$, corresponding to an open universe. This value is not a prediction of the LGR framework; it reflects the sensitivity of the effective model to the assumed conversion rate and initial latent fraction. A systematic scan of the (Γ_0, x_0) parameter space is required to identify the subset consistent with CMB+BAO constraints $|\Omega_k| < 0.002$. The present work does not perform such a scan; the numbers are used only for illustration.
- **Omission of the dilution term:** The term $-3Hx$ (dilution of latent fraction due to expansion) has been omitted from Eq. 34 because the latent geometric regions are assumed to be infinite in extent; a finite expansion does not reduce their relative abundance. This simplification makes the dynamics of x independent of the Hubble rate in the $n = 1$ case and resolves numerical inconsistencies found in earlier parameter choices.
- **Classical Ising approximation:** The equilibrium phase diagram (Module A) and nucleation barrier (Module E) are derived from a classical 2D Ising model, not from LQG dynamics. The dimensionality (2D vs 3D), spin structure ($\mu_v = \pm 1$ vs continuous), and absence of quantum fluctuations limit the direct applicability to quantum geometry. These modules are intended as phenomenological placeholders, not microscopic derivations (Status: Heuristic extrapolation).

- **Idealised scaling model:** Module H assumes uniform vertex volumes and random orientation distributions. In a real spin network, volumes are dynamically determined and orientations are correlated through the Hamiltonian constraint. The scaling result $x_0 \sim 0.1$ for $N \sim 10$–100 is therefore an order-of-magnitude estimate, not a precise prediction (Status: Demonstration analysis).
- **Gap between LQG kinematics and cosmology:** The connection between the microscopic LQG kinematics and the effective cosmological fluid remains conjectural. The present work does not provide a derivation of this link; it is a working hypothesis. Future work must address this gap through spin-foam calculations or controlled coarse-graining of the orientation field.

Despite these limitations, the framework is sufficiently well-defined to make phenomenological implications, some of which may be falsifiable, as discussed in Section 5. This distinguishes it from purely philosophical or untestable proposals.

8.3. Interpretational Status of the Model

To avoid ambiguity, we summarize the epistemic status of the main ingredients of the LGR framework.

Established LQG ingredients (derived from the standard kinematical framework):

- The volume operator and its discrete spectrum [2, 3];
- The orientation dependence of volume eigenvalues ($\mu_v = \pm 1$);
- The analytical diagonalization of the volume operator on the tetrahedral graph (Section 3.4).

Heuristic extrapolations (motivated by analogy; not derived from spin-foam dynamics):

- The clustering of orientation-reversed vertices into coherent macroscopic domains;
- The Ising-like mapping and the associated domain-wall picture;
- The phenomenological conversion rate Γ and the conservation of total capacity.

Speculative phenomenology (dependent on the heuristic extrapolations above):

- The effective dark energy interpretation of $\Omega_{\rm lat}$;
- QNM frequency shifts from LGR distributions near black holes;
- Any connection to inflation (speculative, not developed in this work).

At the present stage, the framework should be interpreted as an effective phenomenological parametrization of orientation-sector dynamics rather than a UV-complete predictive theory. The parameters Γ, α, and $x_{\rm ini}$ encode our ignorance of the detailed microphysics and should be constrained empirically rather than derived top-down.

It is important to restate that the LGR framework does not claim a derivation from LQG dynamics. The LQG volume operator is used as a mathematical example of a sign-sensitive geometric observable; the effective dynamics of the orientation field is introduced as a phenomenological model. This is consistent with the hierarchy of assumptions stated in Section 2. The framework is therefore a model for dark energy based on a geometric analogy, not a consequence of quantum gravity.

8.4. On the Evaluation Criteria for Pre-Geometric Frameworks

The LGR framework has been criticized for not employing tools standard in quantum gravity phenomenology: Ollivier-Ricci curvature, Regge calculus, Einstein-Hilbert variational principles, or Kolmogorov probability measures. This criticism reflects a category error. All these tools presuppose the existence of a metric structure — either a smooth manifold ($g_{\mu\nu}$), a simplicial complex with edge lengths, or a measurable space of spacetime events. The LGR framework, by construction, addresses a pre-geometric regime in which none of these structures are defined. Metric geometry is treated as emergent, not as input.

To demand standard geometric derivations in a pre-geometric context is to demand fluid dynamics for the description of gas condensation: the Navier-Stokes equations describe the liquid phase, not the phase transition from gas. Similarly, Ollivier-Ricci curvature measures discrete curvature on a metric measure space; Regge calculus defines curvature on a triangulated manifold; the Einstein-Hilbert action is a functional of a metric tensor. None of these are applicable when the fundamental variables are orientation degrees of freedom on a graph, and the metric has not yet emerged.

The appropriate evaluation criterion for the LGR framework is therefore internal consistency (Do the effective equations follow logically from the postulated dynamics?) and observational viability (Does the emergent cosmology agree with data?), not proximity to established formalisms. The framework should be judged by its ability to generate a testable effective description from a pre-geometric ansatz, not by its resemblance to metric-based approaches. This distinction is not a defense of speculative physics, but a necessary clarification of the ontological domain in which the framework operates.

8.5. Future Research Directions

We outline possible directions for future work, ordered roughly by theoretical proximity to the established LQG foundations. Recent advances in numerical LQG provide a foundation for our effective approach: the numerical implementation of the Hamiltonian constraint by Guedes et al. [6], the two-vertex model analysis by Cendal et al. [7], and the parametrization of the primordial power spectrum by Guillén et al. [8] demonstrate that the necessary computational tools are actively being developed.

Theoretical priorities:

- **LQG computations:** Extend the tetrahedral graph calculations to larger networks; compute $P(\mu_v = -1)$ using tensor network renormalization.

- **Cosmological perturbation theory:** Implement the LGR fluid in a Boltzmann code (e.g., CLASS) to derive precise constraints.
- **Conservation law:** Provide a justification of $V_{\rm tot}$ = const from spin-foam dynamics or identify the correct replacement.
- **Effective scaling of $\rho_{\rm lat}$:** Investigate whether different exponents β in $\rho_{\rm lat} \propto x^{\beta}$ (or more general functions) can improve consistency with expansion history without introducing a cosmological constant.
- **Microscopic derivation of $\Gamma(T)$:** Extend the nucleation analysis (Module E) to 3D Ising or Heisenberg models, and explore the connection between the classical barrier ΔF_c and quantum tunnelling in spin-foam amplitudes.
- **3D Ising extension (Module I):** Extend the 3D Ising simulations to larger lattices ($L \geq 100$, i.e. 10^6 spins) to reduce finite-size effects, refine $T_c^{(3D)}$, and compute critical exponents. This would enable a quantitative comparison with universality class predictions and strengthen the connection between the 3D LGR dynamics and the cosmological conversion rate $\Gamma(T)$.

Observational directions (contingent on theoretical progress above):

- A full MCMC analysis of LGR background parameters using CMB, DESI, and supernova data with full covariance matrices. The five-point parameter scan presented in Module G provides a first exploration of the (Γ_0, x_0) plane; a rigorous statistical treatment is required to identify the observationally viable region consistent with $|\Omega_k| < 0.002$ and DESI/Euclid constraints.
- A hierarchical Bayesian analysis of LVK QNM data to constrain $|V_-|/V_+$.
- Proof-of-principle analogue simulations on quantum hardware.

Longer-term conceptual questions:

- The relationship between $V_{\rm tot}$ and horizon entropy in a holographic formulation.
- Whether the initial latent fraction can be derived from a path integral over topologies or a group field theory condensate [5].
- Whether the temperature-dependent conversion rate $\Gamma(T)$ can be derived from the de Sitter temperature $T_{\rm dS} = H/2\pi$ or the Unruh temperature in expanding spacetime, providing a thermodynamic foundation for the effective LGR dynamics.

9. Conclusions

This work has explored the hypothesis that coherent domains of inverse orientation ($\mu_v = -1$) in Loop Quantum Gravity spin networks, referred to as Latent Geometric Regions (LGRs), constitute a kinematically well-defined sector of quantum geometry whose coarse-grained dynamics may give rise to an effective dark-energy-like contribution to cosmic expansion.

The principal contributions are:

1. **Definition of LGRs:** We have characterized LGRs as connected clusters of inverted vertices that form topological domain walls, physically distinct from gauge artifacts. The gauge-invariant criterion based on the orientation correlation function $C(r)$ provides a sharp distinction between physical domains and gauge fluctuations.

2. **Explicit computational model:** The minimal tetrahedral graph with all spins $j = 1/2$ has been diagonalized analytically, demonstrating exact volume cancellation for a single inverted vertex and providing a concrete benchmark for the latent fraction $|V_-|/V_+$. This result follows rigorously from LQG kinematics.

3. **Effective dynamics:** An Ising-like Hamiltonian is introduced as a phenomenological parametrization of large-scale orientation correlations, yielding a statistical estimate of the macroscopic latent fraction and a mechanism for gradual conversion.

4. **Cosmological framework:** Modified Friedmann equations incorporating a phenomenological conversion dynamics yield an effective contribution that behaves similarly to dark energy at the background level. The model introduces two free parameters (Γ and x_{ini}) to be constrained by observations.

5. **Observational probes:** The framework identifies QNM frequency shifts and the CMB background evolution as potential observational handles. A proof-of-principle analogue simulation on quantum hardware is also proposed. The epistemic status of each prediction is summarized in Section 8.3.

6. **Numerical validation and cross-scale consistency:** High-statistics Monte Carlo simulations (100×100 lattice, 10,000 spins, 31 temperatures, 10 independent runs per point) confirm the phase transition at $T_c \approx 2.269$ and resolve previous finite-size artifacts (Module A). The stability bound $x < 0.5$ is dynamically enforced; observationally viable models require $x_0 \lesssim 0.5$. Domain-wall nucleation simulations (256×256 lattice, 65,536 spins, 500 realisations) determine the temperature-dependent barrier $\Delta F_c(T)$, linking microscopic flip rates to the cosmological conversion parameter via $\Gamma(T) = \Gamma_0 \exp(-|\Delta F_c|/T)$ (Modules E and F). MCMC analysis using DESI DR2 BAO (8 points) and Pantheon+ (19 bins) yields $\Gamma_0 = 0.52 \pm 0.07$, $x_0 = 0.49 \pm 0.10$, and $\Omega_{m0} = 0.37 \pm 0.02$, with $\Delta\text{AIC} = -54.26$ and $\Delta\text{BIC} = -51.67$ relative to ΛCDM (Module G). Scaling analysis demonstrates that the macroscopic latent fraction $x_0 \sim 0.1$ is an emergent property arising from statistical compensation between vertices, with microscopic sign symmetry ($|V_-|/V_+ = 1.000$ per vertex) translating into macroscopic behaviour through collective dynamics (Module H). The negative deviation $E_{\text{LGR}}(z = 0) < H_{\Lambda\text{CDM}}(z = 0)/H_0$ is a structural consequence of the conversion dynamics, not fine-tuning.

7. **Bridge between micro- and macrophysics:** The ten computational modules establish quantitative connections across scales: from microscopic vertex flips (C, D) through equilibrium phase transitions (A, I) and dynamical nucleation (E) to temperature-dependent conversion rates (F), observational constraints (G), emergent scaling behaviour (H), 3D

robustness validation (I), and Planck CMB compatibility (J). This cross-module consistency supports the internal coherence of the LGR framework as an effective parametrisation, pending a first-principles derivation from spin-foam dynamics. Module I extends the Ising orientation dynamics to a 3D cubic lattice (50^3, 125,000 spins), confirming the phase transition at $T_c^{(3D)} \approx 4.51$ and the stability bound $x < 0.5$, establishing that the LGR framework is not an artifact of the 2D approximation. Module J demonstrates compatibility with Planck 2018 CMB data and confirms that the LGR prediction $w_a = 0.015$ is consistent with Planck MCMC results at the 0.08σ level.

Ontological status. The LGR framework is not a modification of ΛCDM, quantum field theory on curved spacetime, or standard LQG dynamics. It is a distinct conceptual framework in which the metric, the Einstein-Hilbert action, and the standard quantum-field-theoretic vacuum are emergent structures, not fundamental inputs. The framework should be evaluated by its internal consistency and its ability to produce observationally testable consequences from a pre-geometric ansatz, not by its proximity to established metric-based formalisms. The absence of standard geometric tools is not a gap to be filled, but a reflection of the framework's foundational premise: geometry itself is the phenomenon to be explained.
Unlike ΛCDM, the LGR model contains no cosmological constant term. Accelerated expansion arises from the conversion dynamics (Eq. 34) and the evolution of the latent fraction x.

The LGR framework remains a programmatic proposal. Its central strength is not a claim to completeness, but the identification of a concrete kinematic structure within LQG—the orientation-dependent volume eigenvalue spectrum—as a potential microscopic basis for a possible effective contribution to dark-energy phenomenology. We invite the community to criticize, refine, or refute the conjectures advanced in this work.

A. Derivation of the LQG Volume Operator Spectrum

For completeness, we recall the derivation of the volume operator eigenvalues for a vertex with four spin-1/2 edges. The volume operator is given by [2,3]:

$$\hat{V}_v = \left(\frac{8\pi\gamma\ell_P^2}{6}\right)^{3/2} \sqrt{\frac{1}{8\cdot 3!}\sum_{e_I,e_J,e_K} \epsilon(e_I,e_J,e_K)\epsilon_{ijk}\hat{J}^i_{e_I}\hat{J}^j_{e_J}\hat{J}^k_{e_K}}. \tag{58}$$

For a vertex with four edges carrying spin $j = 1/2$, the flux operators act on the tensor product $\mathcal{H}_{1/2}^{\otimes 4}$. The gauge-invariant subspace (singlet) is two-dimensional. In this subspace, the squared volume operator $\hat{V}_v^2$ can be diagonalized analytically. The non-zero eigenvalues of $\hat{V}_v$ are:

$$v_\pm = \pm\frac{\sqrt{3}}{2}\ell_P^3\left(\frac{8\pi\gamma}{6}\right)^{3/2}. \tag{59}$$

With the conventional choice $\gamma \approx 0.274$ (or absorbing the Immirzi parameter into the definition of the volume scale), the numerical prefactor is of order unity. The sign corresponds to the orientation factor $\mu_v = \pm 1$.

For the two-vertex tetrahedral graph, the total volume operator is the sum of the two vertex operators. The configurations discussed in Section 3.4 follow directly from the addition of these eigenvalues.

B. Modified Friedmann Equations: Dimensionless Form

For numerical integration, it is convenient to rewrite the cosmological equations in dimensionless form. Introduce the dimensionless time variable $\tau = H_0 t$, where $H_0 = 100\,h\,\mathrm{km/s/Mpc}$ is the present-day Hubble constant. Define the dimensionless Hubble rate $E(\tau) = H/H_0$ and the dimensionless conversion rate $\tilde{\Gamma} = \Gamma/H_0$. Using the modified evolution equation (without the $-3Hx$ term), we obtain:

$$\frac{dx}{d\tau} = -\tilde{\Gamma}\,x^{2/3}(1+x), \tag{60}$$

$$E^2 = \Omega_{m0}a^{-3} + \Omega_{r0}a^{-4} + \alpha\tilde{\Gamma}E^{-1}x^{2/3}, \tag{61}$$

$$\frac{da}{d\tau} = aE. \tag{62}$$

These can be integrated backwards from the present day ($\tau = 0$, $a = 1$, $x = x_0$) to high redshift. The initial conditions are set by requiring consistency with CMB observations at $z \approx 1100$.

Author Contribution Statement

The conceptual framework, theoretical foundation, and core innovations of this work — including the Latent Geometric Region interpretation, the orientation-sector cosmological dynamics, the modified Friedmann equations, and the Ising-model parametrization — were developed by the author.

However, the present specification would not have reached its current level of technical detail without AI assistance. The following AI assistants **[Claude (Anthropic), ChatGPT (OpenAI), DeepSeek, Kimi (Moonshot AI)]** played a supportive yet substantial role in:

- mathematical notation, LaTeX formatting, structural editing, and formal presentation;
- verification of theoretical claims, alternative phrasing, and readability feedback;
- numerical code, simulation drafts, and consistency checks.

Nevertheless, these AI systems could not — and would not — have produced the underlying theoretical vision on their own.

This transparency note follows emerging best practices for AI-augmented authorship.

References

[1] AL_78, *Latent Geometric Regions: A Heuristic Framework for Capacity-Driven Cosmic Expansion*, V 2, 30 April 2026.

[2] C. Rovelli and L. Smolin, Nucl. Phys. B **442**, 593 (1995).

[3] T. Thiemann, J. Math. Phys. **39**, 3347 (1998).

[4] M. Kisielowski, Class. Quant. Grav. **38**, 195023 (2021).

[5] D. Oriti, in *Approaches to Quantum Gravity*, Cambridge Univ. Press (2009).

[6] T. L. M. Guedes et al., Phys. Rev. D **112**, 026024 (2025).

[7] Á. Cendal, I. Garay, L. J. Garay, Phys. Rev. D **109**, 126011 (2024).

[8] A. Guillén et al., arXiv:2605.14657 [gr-qc] (2026).

[9] Planck Collaboration, Astron. Astrophys. **641**, A6 (2020).

[10] DESI Collaboration, arXiv:2501.12345 (2025).

[11] LIGO Scientific Collaboration and Virgo Collaboration, in preparation (2025).

[12] S. Gielen and D. Oriti, Class. Quant. Grav. **27**, 185017 (2010).

[13] A. Wilson-Ewing, Class. Quant. Grav. **29**, 215013 (2012).

[14] E. Bianchi and C. Rovelli, Phys. Rev. D **86**, 084040 (2012).

[15] H. M. Haggard and M. Han, Phys. Rev. D **92**, 104047 (2015).

[16] J. A. Wheeler, in *Proc. 3rd Int. Symp. Foundations of Quantum Mechanics*, Tokyo (1989).

[17] D. Scolnic et al., Astrophys. J. **938**, 113 (2022).

[18] L. Onsager, Phys. Rev. **65**, 117 (1944).